

# Learnable Koopman-Enhanced Transformer-Based Time Series Forecasting with Spectral Control

Ali Forootani\*, Senior Member, IEEE, Raffaele Iervolino, Senior Member, IEEE,

**Abstract**—This paper proposes a unified family of learnable Koopman operator parameterizations that integrate linear dynamical systems theory with modern deep learning forecasting architectures. We introduce four learnable Koopman variants—scalar-gated, per-mode gated, MLP-shaped spectral mapping, and low-rank Koopman operators—which generalize and interpolate between strictly stable Koopman operators and unconstrained linear latent dynamics. Our formulation enables explicit control over the spectrum, stability, and rank of the linear transition operator while retaining compatibility with expressive nonlinear backbones such as PatchTST, Autoformer, and Informer.

We evaluate the proposed operators in a large-scale benchmark that also includes LSTM, DLinear, and simple diagonal State-Space Models (SSMs), as well as lightweight transformer variants. Experiments across multiple horizons and patch lengths show that learnable Koopman models provide a favorable bias-variance trade-off, improved conditioning, and more interpretable latent dynamics. We provide a full spectral analysis, including eigenvalue trajectories, stability envelopes, and learned spectral distributions. Our results demonstrate that learnable Koopman operators are effective, stable, and theoretically principled components for deep forecasting.

**Index Terms**—Time Series Forecasting, Transformer Models, Autoformer, Informer, PatchTST, Koopman Operator.

## I. INTRODUCTION

Time series forecasting is a foundational task across science and engineering, underpinning applications in retail demand prediction [1], [2], [3], traffic flow management [4], [5], energy balancing [6], [7], [8], and financial volatility modeling [9], [10]. The increasing scale, dimensionality, and non-stationarity of modern datasets challenge traditional statistical models [11], driving the development of deep learning architectures that offer improved expressiveness, scalability, and feature abstraction.

Early deep learning models such as RNNs and LSTMs [12], [3], as well as CNN and TCN architectures [13], [14], demonstrated strong forecasting capabilities by learning temporal dependencies directly from data. More recently, Transformer-based architectures [15], [16], [17], [18] have become the dominant paradigm due to their ability to model long-range dependencies via self-attention. Their effectiveness has been validated in large-scale forecasting competitions such as M4 and M5 [19], [20].

To improve scalability and accuracy, numerous specialized Transformers have been proposed. Informer [21], [16]

Ali Forootani is with Max Planck Institute of Geoanthropology Kahlaische Str. 10, 07745 Jena, Germany (email: forootani@gea.mpg.de/aliforootani@ieee.org).

Raffaele Iervolino is with Department of Electrical Engineering and Information Technology, University of Naples, 80125 Napoli, Italy (email: rafiev@unina.it).

introduces ProbSparse attention to focus on the most informative queries; Autoformer [22], [15] integrates decomposition blocks to explicitly handle trend and seasonal patterns; FEDformer [23], [24] employs Fourier spectral mixing to reduce complexity; and Pyraformer [25], [26] introduces a pyramidal hierarchy to capture multi-scale structures. More recently, PatchTST [17] showed that simple architectural principles—patching, channel-independence, and lightweight attention—are sufficient to outperform many deeper Transformer variants [27], [28].

Following the surprising results of DLinear [28], [29], which showed that a channel-wise linear model can outperform many Transformers on standard benchmarks, a central question has emerged: *how much architectural complexity is actually necessary for strong time-series forecasting performance?* Moreover, deep models still suffer from limited interpretability, sensitivity to distribution shifts [30], [31], [32], and a lack of explicit dynamical structure, limiting their robustness in high-stakes settings.

To address these issues, recent research has sought to embed domain priors and system dynamics into learning architectures. Hybrid statistical-deep models [33], [34], [19], continuous-time neural ODE frameworks [35], [36], and physics-inspired models aim to introduce structural inductive biases. However, many such approaches still require strong assumptions on fixed dynamics and face scalability challenges in multivariate or highly nonlinear environments.

## A. Koopman Operators and Deep Learning

The *Koopman operator* offers a linear lens for analyzing nonlinear dynamical systems by evolving observables rather than states. Formally, it is an infinite-dimensional linear operator acting on functions of the state, enabling the use of linear spectral tools in settings that may be nonlinear, nonstationary, or even chaotic [37], [38]. Classical data-driven approaches such as Dynamic Mode Decomposition (DMD) approximate the Koopman spectrum for prediction and modal analysis [39], [40], but tend to degrade under high-dimensional, noisy, or multivariate real-world data. Dynamic Mode Decomposition (DMD) offer practical means to approximate the operator from measurements and facilitate modal analysis, prediction, and control in complex systems [41], [42], [43].

Deep learning has revitalized Koopman theory by learning nonlinear embeddings in which latent dynamics evolve linearly. Neural Koopman models typically employ an encoder  $\mathcal{E}_\theta$  to produce latent coordinates  $z_t = \mathcal{E}_\theta(X_t)$  from an input window  $X_t$ , and a linear propagator  $z_{t+1} = \mathcal{K}z_t$ , often coupled with nonlinear decoders, spectral regularization, and

stability constraints [44], [45], [46], [47], [48], [49], [50]. These advances have led to interpretable and stable rollout predictions, with recent extensions exploring low-rank structure, symmetry priors, and multiresolution latent spaces [51]. However, most architectures rely on shallow networks and struggle to model long-range, non-local temporal dependencies that modern Transformer-based models address effectively.

Recent work has begun incorporating Koopman operators into Transformer architectures to obtain stable and interpretable latent dynamics, so called DeepKoopFormer[52].

Compared to existing Koopman-based forecasting models [47], [50], [48], DeepKoopFormer is the first to offer provable spectral decay, Lyapunov-stable propagation, normality of the transition matrix, and closed-form error control—all within a general, extensible encoder–propagator–decoder pipeline aligned with the goals of physics-informed forecasting [53], [54] and interpretable dynamical systems modeling [55], [56].

### B. Contributions: Learnable Koopman–Transformer Framework

Although initial results demonstrate strong potential, most existing designs rely on fixed or heavily constrained Koopman operators, leaving a large space of learnable operator parameterizations largely unexplored. Indeed, existing Koopman–neural models typically combine nonlinear feature encoders with a latent linear operator [50], [47]. However, the operator itself is usually learned *without explicit spectral parameterization*: it is fitted as an unconstrained linear layer or least-squares estimator, providing no mechanism to shape contraction, oscillation, or multi-scale temporal behavior. Moreover, such formulations have rarely been integrated with modern Transformer architectures, despite their demonstrated ability to model long-range dependencies in time series. This combination of *spectral non-control* and *architectural underuse* limits both interpretability and dynamical expressiveness.

To address these limitations, we introduce the Learnable–DeepKoopFormer, a unified framework that equips Transformer backbones with *parameterized Koopman operators* whose spectra are learned directly from data. Our formulation includes four operator families:

- **scalar-gated:** global trainable parameters  $(\alpha, \beta)$  control spectral shifting and scaling, enabling tunable damping or persistent dynamics;
- **per-mode gated:** dimension-wise parameters  $(\alpha_i, \beta_i)$  model anisotropic temporal responses and multi-frequency evolution;
- **MLP-shaped spectral mapping:** neural spectral mappings are projected onto stable linear propagators with controlled spectral radius;
- **low-rank Koopman:** relatively low rank factorizations of the Koopman operator to capture high-dimensional latent dynamics efficiently through structured compression.

These operator designs are embedded into lightweight and full Transformer forecasters, including PatchTST [17], Informer [16], and Autoformer [15], yielding a comprehensive family of DeepKoopFormer models. Spectral stability constraints and operator regularization allow latent

dynamics to be jointly optimized with representation learning while preserving interpretability: the dominant modes, stability margins, and spectral envelopes remain directly analyzable.

We conduct an extensive simulation benchmark comparing the proposed learnable Koopman variants against two reference Koopman baselines—a spectrally constrained variant and an unconstrained variant—together with widely used forecasting models including LSTM, DLinear [28], [29], and a diagonal State-Space Model (SSM) [57]. Alongside forecasting accuracy, we provide the first systematic *spectral evaluation* of Koopman–Transformers, including density characterization, eigenvalue training trajectories, stability envelopes, and horizon sensitivity.

In summary, this work provides:

- a unified parameterization of *learnable Koopman operators* (scalar, per-mode, neural, and low-rank);
- the Learnable–DeepKoopFormer framework, embedding these operators into three state-of-the-art Transformer backbones;
- a systematic benchmark of 21 *models* across constrained, learnable, and unconstrained variants, plus LSTM, DLinear, and diagonal SSM baselines;
- the first comprehensive *spectral analysis of Koopman–Transformer models*, revealing stability properties, multi-scale expressiveness, and interpretable latent dynamics.

For real-world evaluation, we utilize high-dimensional datasets from multiple domains, including: the CMIP6 climate projections <sup>1</sup> and ERA5 reanalysis data <sup>2</sup>, focusing on wind speed and surface pressure forecasting over Germany; a financial time series dataset <sup>3</sup> for cryptocurrency market analysis; and an electricity generation dataset <sup>4</sup> for modeling energy supply dynamics. These datasets collectively span chaotic, periodic, and stochastic regimes, allowing for a comprehensive assessment of model accuracy, stability, and generalization across domains.

Compared to existing Koopman-based forecasting models [47], [50], [48], Learnable–DeepKoopFormer is the first to offer provable spectral decay, Lyapunov-stable propagation, normality of the transition matrix, and closed-form error control—all within a general, extensible encoder–propagator–decoder pipeline aligned with the goals of physics-informed forecasting [53], [54] and interpretable dynamical systems modeling [55], [56].

This paper is organized as follows. Section II provides the preliminaries required for time series forecasting. In Section III, we present Learnable–DeepKoopFormer architectures for multivariate time series forecasting. Numerical simulations are presented in Section IV to evaluate the performance of Learnable–DeepKoopFormer versus other benchmarks. Finally, we conclude the article in Section V.

<sup>1</sup><https://cds.climate.copernicus.eu/datasets/projections-cordex-domains-single-levels?tab=overview>

<sup>2</sup><https://cds.climate.copernicus.eu/datasets>

<sup>3</sup><https://github.com/Chisomnwa/Cryptocurrency-Data-Analysis>

<sup>4</sup><https://github.com/afshinfaramarzi/Energy-Demand-electricity-price-Forecasting/tree/main>

## II. LEARNABLE-DEEPKOOPFORMER ARCHITECTURE

We begin by formalizing the multivariate time series forecasting task and introducing the key components of the proposed architecture.

Given a multivariate time series  $\{x_t\}_{t=1}^T$ , with  $x_t \in \mathbb{R}^{d_s}$ , Learnable-DeepKoopFormer operates on context windows of length  $P$  and predicts the subsequent  $H$  samples. For each valid index  $t$ , an input segment  $X_t = [x_t, \dots, x_{t+P-1}] \in \mathbb{R}^{P \times d_s}$  is paired with its future sequence  $Y_t = [x_{t+P}, \dots, x_{t+P+H-1}] \in \mathbb{R}^{H \times d_s}$ . The input window is passed through a Transformer encoder with positional encoding  $\mathcal{E}_\theta$  (e.g., PatchTST, Autoformer, or Informer), producing a latent representation

$$z_t = \mathcal{E}_\theta(X_t) \in \mathbb{R}^{d_{\text{lat}}},$$

where  $d_{\text{lat}}$  is the latent dimension. Typically  $d_{\text{lat}} = d_{\text{model}}$ , and not necessarily equal to the physical dimension  $d_s$ , where  $d_{\text{model}}$  denotes the hidden (embedding) dimension of the Transformer backbone, i.e., the dimensionality of the token representations and of the latent state produced by the encoder  $\mathcal{E}_\theta$ . With the slight abuse of notation and for the sake of simplicity, hereinafter we assume  $d_{\text{model}} = d_{\text{lat}} = d_s = d$ .

Temporal evolution in the latent space is modeled through a learned Koopman operator  $\mathcal{K}_\phi$ , which advances the latent state linearly according to  $z_{t+1} = \mathcal{K}_\phi z_t$ . The propagated latent state is decoded into a direct  $H$ -step forecast using a linear mapping  $\mathcal{D}_\varphi$ , yielding a vector  $\hat{y}_t = \mathcal{D}_\varphi(z_{t+1}) \in \mathbb{R}^{H \times d}$ , which is then reshaped into the output sequence  $\hat{Y}_t \in \mathbb{R}^{H \times d}$ .

Here, the subscript  $\theta$  denotes the parameters of the Transformer encoder  $\mathcal{E}_\theta$ ,  $\phi$  collects the parameters of the Koopman propagator  $\mathcal{K}_\phi$  (including its spectral coefficients and orthogonal factors), and  $\varphi$  denotes the parameters of the linear decoder  $\mathcal{D}_\varphi$ . During inference, a context window  $X_t$  is encoded once, propagated through the Koopman operator  $\mathcal{K}_\phi$ , and decoded to produce the entire prediction horizon  $H$  in a single forward pass, without autoregressive rollout.

All components are trained jointly in an end-to-end fashion using the Adam optimizer [58], a first-order stochastic gradient method with adaptive moment estimation. In particular, training is performed end-to-end by minimizing a forecasting loss (e.g., mean squared error) augmented with a Lyapunov-inspired penalty as follows

$$\begin{aligned} \mathcal{L} &= \mathbb{E} \left[ \|\hat{Y}_t - Y_t\|^2 \right] + \lambda_{\text{Lyap}} \mathbb{E} \left[ \|\mathcal{K}_\phi z_t\|_P^2 - \|z_t\|_P^2 \right]_+ \\ &= \mathcal{L}_{\text{MSE}} + \lambda_{\text{Lyap}} \mathcal{L}_{\text{Lyap}}, \end{aligned} \quad (1)$$

where  $\|z\|_P^2 = z^\top P z$ ,  $P \succ 0$  is a fixed positive-definite matrix,  $[x]_+ = \max\{x, 0\}$ , and  $\lambda_{\text{Lyap}} > 0$  is a scalar regularization weight controlling the strength of the Lyapunov stability penalty.

## III. LEARNABLE KOOPMAN VARIANTS

In Learnable-DeepKoopFormer we assume the latent evolution to be modeled by a linear dynamics through a learned Koopman propagator  $\mathcal{K}_\phi \in \mathbb{R}^{d \times d}$ ,

$$z_{t+1} = \mathcal{K}_\phi z_t.$$

As shown later in the paper, to ensure identifiability and stable training,  $\mathcal{K}_\phi$  is parameterized through an orthogonal-diagonal-orthogonal (ODO) factorization

$$\mathcal{K}_\phi = U_\phi \text{diag}(\Sigma_\phi) V_\phi^\top, \quad (2)$$

where  $U_\phi, V_\phi$  are learned orthonormal matrices obtained via QR retraction, and  $\Sigma_\phi = (\Sigma_{\phi,1}, \dots, \Sigma_{\phi,d})^\top \in \mathbb{R}^d$  (or  $\mathbb{R}^r$  in the low-rank case, see later in the paper) the vector containing the learnable spectral coefficients. Equation (2) ensures that all nonlinearity and expressiveness are concentrated in the spectrum  $\Sigma_\phi$ , while the left/right singular directions evolve on the Stiefel manifold, i.e., the set of matrices with orthonormal columns [59].

The key design freedom of our *learnable Koopman architecture* lies in how the diagonal spectral coefficients  $\Sigma_\phi$  are generated. We consider Koopman variants that share the principle

$$\Sigma_{\phi,i} = \rho_{\max} \sigma_\phi(S_i), \quad i = 1, \dots, d, \quad (3)$$

where  $S_i \in \mathbb{R}$  are raw trainable parameters,  $\rho_{\max} \in (0, 1)$  is a prescribed spectral bound, and  $\sigma_\phi(\cdot)$  is a smooth squashing map, i.e. a nonlinear “spectral shaping” function, which preserves differentiability and enables end-to-end learning while providing explicit control over contraction rates in the latent Koopman dynamics. This map is chosen to enforce

$$|\Sigma_{\phi,i}| < \rho_{\max} \quad \text{for all } i, \quad \rho_{\max} \in (0, 1), \quad (4)$$

whenever spectral stability is desired, while allowing different degrees of expressiveness. In particular, it is the composition of the logistic sigmoid  $\sigma(x) = \frac{1}{1+e^{-x}}$  and a function chosen from a list of spectral shaping maps. More specifically, we introduce four learnable Koopman families that act on the vector of raw spectral parameters

- 1) **scalar-gated.** A shared affine gate controls the entire spectrum:

$$\sigma_\phi(S_i) = \sigma(\alpha S_i + \beta), \quad (5)$$

with  $\alpha, \beta \in \mathbb{R}$  learned scalars.

- 2) **per-mode gated.** Each latent direction receives its own gate,

$$\sigma_\phi(S_i) = \sigma(\alpha_i S_i + \beta_i), \quad (6)$$

allowing anisotropic amplification/decay across modes.

- 3) **MLP-shaped spectral mapping.** A small neural operator  $g_\phi : \mathbb{R} \rightarrow \mathbb{R}$  transforms raw spectral parameters before squashing:

$$\sigma_\phi(S_i) = \sigma(g_\phi(S_i)), \quad (7)$$

enabling flexible nonlinear reshaping of the spectrum.

- 4) **low-rank Koopman.** The operator is restricted to rank  $r \ll d$  via

$$\mathcal{K}_\phi = U_{r,\phi} \text{diag}(\Sigma_{r,\phi}) V_{r,\phi}^\top, \quad U_{r,\phi}, V_{r,\phi} \in \mathbb{R}^{d \times r}, \quad (8)$$

with orthonormal columns and a spectral vector  $\Sigma_{r,\phi} \in \mathbb{R}^r$  satisfying again  $|\Sigma_{r,\phi,i}| < \rho_{\max}$ . It encourages low-dimensional latent dynamics and reduces complexity.

In addition, for comparison purpose, we also consider a fully free operator (unconstrained baseline) obtained when  $\mathcal{K}_\phi$  is a

free dense matrix, without the ODO structure (2) and without the spectral bound (4). This variant maximizes expressiveness but lacks the stability and dynamical bias of the structured families above.  $\blacksquare$

Overall, the learnable Koopman architecture provides a continuum between rigorously constrained operator-theoretic propagators and fully flexible data-driven linear maps, allowing us to isolate and study the role of spectral structure in Transformer-based forecasting models.

### A. Theoretical Properties of the Learnable Koopman Propagator

We consider latent states  $z_t \in \mathbb{R}^d$  evolving under a linear propagator

$$z_{t+1} = \mathcal{K}_\phi z_t, \quad \mathcal{K}_\phi \in \mathbb{R}^{d \times d}, \quad (9)$$

where  $\mathcal{K}_\phi$  is parameterized by the learnable weights  $\phi$  of the Koopman module in DeepKoopFormer. This subsection collects several structural properties of the proposed parameterizations, focusing on stability, expressiveness, low-rank structure, and Lyapunov regularization.

1) *Spectral stability, contraction, and invertibility:* The spectral bound (4) directly implies stability and contractivity of the associated linear dynamics.

*Proposition 1 (Spectral stability):* Let  $\mathcal{K}_\phi$  be parameterized as in (2), with orthonormal  $U_\phi, V_\phi$  and diagonal  $\text{diag}(\Sigma_\phi)$  satisfying (4). Then

$$\rho(\mathcal{K}_\phi) \leq \|\mathcal{K}_\phi\|_2 = \max_i |\Sigma_{\phi,i}| < \rho_{\max}, \quad (10)$$

where  $\rho(\cdot)$  denotes the spectral radius and  $\|\cdot\|_2$  the spectral norm.

*Proof:* Because  $U_\phi$  and  $V_\phi$  are orthonormal, left and right multiplication do not change the spectral norm:

$$\|\mathcal{K}_\phi\|_2 = \|U_\phi \text{diag}(\Sigma_\phi) V_\phi^\top\|_2 = \|\text{diag}(\Sigma_\phi)\|_2. \quad (11)$$

The spectral norm of a diagonal matrix is the maximum absolute diagonal entry, hence

$$\|\mathcal{K}_\phi\|_2 = \max_i |\Sigma_{\phi,i}|. \quad (12)$$

For any matrix, the spectral radius is bounded above by the spectral norm,  $\rho(\mathcal{K}_\phi) \leq \|\mathcal{K}_\phi\|_2$ . Combining this with  $|\Sigma_{\phi,i}| < \rho_{\max}$  for all  $i$  yields the claim.  $\blacksquare$

*Corollary 1 (Exponential contraction in latent space):*

Under the assumptions of Proposition 1, for any  $z_0 \in \mathbb{R}^d$  and any  $n \in \mathbb{N}$ ,

$$\|\mathcal{K}_\phi^n z_0\|_2 \leq \|\mathcal{K}_\phi\|_2^n \|z_0\|_2 \leq \rho_{\max}^n \|z_0\|_2, \quad (13)$$

and hence  $\lim_{n \rightarrow \infty} \mathcal{K}_\phi^n z_0 = 0$ .

*Proof:* Submultiplicativity of the spectral norm gives  $\|\mathcal{K}_\phi^n\|_2 \leq \|\mathcal{K}_\phi\|_2^n$ , so

$$\|\mathcal{K}_\phi^n z_0\|_2 \leq \|\mathcal{K}_\phi\|_2^n \|z_0\|_2 \leq \|\mathcal{K}_\phi\|_2^n \|z_0\|_2. \quad (14)$$

Proposition 1 implies  $\|\mathcal{K}_\phi\|_2 < \rho_{\max} < 1$ , hence the right-hand side converges to zero as  $n \rightarrow \infty$ , i.e. the latent dynamics (9) is exponentially stable:

$$\|z_t\|_2 \leq \rho_{\max}^t \|z_0\|_2, \quad t \geq 0. \quad (15)$$

In many forecasting settings, it is also natural to consider the inverse dynamics whenever the spectrum is bounded away from zero. This leads to the following simple consequence of the ODO structure.  $\blacksquare$

*Proposition 2 (Invertibility and stability of the inverse):* Assume the ODO parameterization (2) satisfies the two-sided spectral bound

$$0 < \rho_{\min} \leq |\Sigma_{\phi,i}| \leq \rho_{\max} < 1 \quad \text{for all } i. \quad (16)$$

Then  $\mathcal{K}_\phi$  is invertible with

$$\mathcal{K}_\phi^{-1} = V_\phi \text{diag}(\Sigma_{\phi,1}^{-1}, \dots, \Sigma_{\phi,d}^{-1}) U_\phi^\top, \quad (17)$$

and

$$\rho(\mathcal{K}_\phi^{-1}) \leq \|\mathcal{K}_\phi^{-1}\|_2 = \max_i |\Sigma_{\phi,i}^{-1}| \leq \rho_{\min}^{-1}. \quad (18)$$

*Proof:* Under (16), all diagonal entries of  $\text{diag}(\Sigma_\phi)$  are nonzero, so it is invertible. Since  $U_\phi$  and  $V_\phi$  are orthonormal,  $\mathcal{K}_\phi$  is invertible and its inverse has the stated form. The spectral norm calculation proceeds exactly as in Proposition 1, yielding  $\|\mathcal{K}_\phi^{-1}\|_2 = \max_i |\Sigma_{\phi,i}^{-1}|$ , and  $\rho(\mathcal{K}_\phi^{-1}) \leq \|\mathcal{K}_\phi^{-1}\|_2$ .  $\blacksquare$

This shows that the same spectral factors that enforce forward-time contraction can also guarantee that the inverse dynamics are well-conditioned, provided the spectrum is kept away from zero.

2) *Expressiveness of spectrally bounded and low-rank operators:* The ODO factorization parameterizes exactly the class of linearly stable operators with bounded spectral norm.

*Proposition 3 (Representation of all spectrally bounded operators):* Fix  $\rho_{\max} > 0$  and define

$$\mathcal{K}(\rho_{\max}) := \left\{ \mathcal{K} \in \mathbb{R}^{d \times d} : \|\mathcal{K}\|_2 \leq \rho_{\max} \right\}. \quad (19)$$

Then the set of matrices that admit an ODO factorization with  $|\Sigma_{\phi,i}| \leq \rho_{\max}$  is precisely  $\mathcal{K}(\rho_{\max})$ . In particular, any  $\mathcal{K}$  with  $\|\mathcal{K}\|_2 < \rho_{\max}$  can be represented exactly by some choice of  $(U_\phi, V_\phi, \Sigma_\phi)$ .

*Proof:* (*Surjectivity onto  $\mathcal{K}(\rho_{\max})$ .*) Let  $\mathcal{K} \in \mathcal{K}(\rho_{\max})$ . By the singular value decomposition, there exist orthonormal matrices  $U, V \in \mathbb{R}^{d \times d}$  and nonnegative singular values  $\Sigma_1, \dots, \Sigma_d$  such that

$$\mathcal{K} = U \text{diag}(\Sigma_1, \dots, \Sigma_d) V^\top. \quad (20)$$

The spectral norm is  $\|\mathcal{K}\|_2 = \max_i \Sigma_i$ , so  $\|\mathcal{K}\|_2 \leq \rho_{\max}$  implies  $\Sigma_i \leq \rho_{\max}$  for all  $i$ . Thus  $\mathcal{K}$  admits an ODO factorization with  $U_\phi = U$ ,  $V_\phi = V$  and  $\Sigma_{\phi,i} = \Sigma_i$  satisfying  $|\Sigma_{\phi,i}| \leq \rho_{\max}$ .

*(Inclusion in  $\mathcal{K}(\rho_{\max})$ .)* Conversely, let  $\mathcal{K}_\phi = U_\phi \text{diag}(\Sigma_\phi) V_\phi^\top$  with  $\max_i |\Sigma_{\phi,i}| \leq \rho_{\max}$ . As in the proof of Proposition 1,

$$\|\mathcal{K}_\phi\|_2 = \|\text{diag}(\Sigma_\phi)\|_2 = \max_i |\Sigma_{\phi,i}| \leq \rho_{\max}, \quad (21)$$

hence  $\mathcal{K}_\phi \in \mathcal{K}(\rho_{\max})$ .  $\blacksquare$

Thus the strictly stable and learnable Koopman variants with  $|\Sigma_{\phi,i}| < \rho_{\max}$  retain the full expressiveness of all linear operators in the spectrally bounded class  $\mathcal{K}(\rho_{\max})$ , while providing an explicit stability margin.

3) *Low-rank structure and approximation*: For the low-rank family (8), the Koopman operator is restricted to a rank- $r$  subspace of  $\mathbb{R}^d$ .

*Proposition 4 (Low-rank structure and norm bound):* For the low-rank Koopman parameterization (8):

- 1)  $\text{rank}(\mathcal{K}_\phi) \leq r$ ;
- 2)  $\|\mathcal{K}_\phi\|_2 = \max_{i \leq r} |\Sigma_{r,\phi,i}|$ ;
- 3) if  $|\Sigma_{r,\phi,i}| < \rho_{\max}$  for all  $i$ , then  $\rho(\mathcal{K}_\phi) \leq \|\mathcal{K}_\phi\|_2 < \rho_{\max}$ .

*Proof:* (1) The product of a  $d \times r$  matrix, an  $r \times r$  diagonal matrix and an  $r \times d$  matrix has rank at most  $r$ . (2) Since  $U_{r,\phi}$  and  $V_{r,\phi}$  have orthonormal columns, they describe partial isometries from  $\mathbb{R}^r$  into  $\mathbb{R}^d$ , and the nonzero singular values of  $\mathcal{K}_\phi$  coincide with the absolute values of the entries of  $\Sigma_{r,\phi}$ . Hence  $\|\mathcal{K}_\phi\|_2 = \max_{i \leq r} |\Sigma_{r,\phi,i}|$ . (3) The last claim follows from (2) together with  $\rho(\mathcal{K}_\phi) \leq \|\mathcal{K}_\phi\|_2$  and the bound  $|\Sigma_{r,\phi,i}| < \rho_{\max}$ .  $\blacksquare$

Let  $\mathcal{K}_\phi$  have singular values  $\Sigma_{\phi,1} \geq \dots \geq \Sigma_{\phi,d} \geq 0$ , and let  $\mathcal{K}_\phi^{(r)}$  denote the truncation of its singular value decomposition to rank  $r$ , i.e.,  $\mathcal{K}_\phi^{(r)}$  retains only the first  $r$  singular values and vectors. The Eckart–Young theorem (see [60] for more details) states that  $\mathcal{K}_\phi^{(r)}$  minimizes  $\|\mathcal{K}_\phi - \tilde{\mathcal{K}}_\phi\|_F$  over all rank- $r$  matrices  $\tilde{\mathcal{K}}_\phi$ . Any such  $\mathcal{K}_\phi^{(r)}$  admits a representation of the form (8), and thus belongs to the low-rank family. Consequently, whenever the latent Koopman dynamics are approximately low-dimensional, the low-rank variant can capture the principal modes while discarding high-rank noise.

4) *Lyapunov regularization and energy decay*: Besides spectral constraints, the training objective incorporates in (1) a Lyapunov-inspired penalty that encourages contractive behavior with respect to a fixed quadratic form. For latent pairs  $(\mathbf{z}_t, \mathbf{z}_{t+1})$  the addition of the term

$$\mathcal{L}_{\text{Lyap}} = \mathbb{E} \left[ (\|\mathbf{z}_{t+1}\|_P^2 - \|\mathbf{z}_t\|_P^2)_+ \right], \quad \|\mathbf{z}\|_P^2 = \mathbf{z}^\top P \mathbf{z}, \quad (22)$$

with  $(x)_+ = \max\{x, 0\}$  and  $P \succ 0$ , provides a common regularizer across learnable, Koopman variants, which further biases optimisation toward strict contraction of latent energy by penalizing unstable latent growth and promoting Koopman-consistent dynamics. The following results formalize these considerations.

*Proposition 5 (Lyapunov consistency):* Suppose  $P \succ 0$  and the support of  $\mathbf{z}_t$  spans  $\mathbb{R}^d$ . If  $\mathcal{L}_{\text{Lyap}} = 0$ , then  $\mathcal{K}_\phi$  satisfies the discrete Lyapunov inequality

$$\mathcal{K}_\phi^\top P \mathcal{K}_\phi - P \preceq 0. \quad (23)$$

In particular, the quadratic energy  $\|\mathbf{z}_t\|_P^2$  is non-increasing under the dynamics  $\mathbf{z}_{t+1} = \mathcal{K}_\phi \mathbf{z}_t$ .

*Proof:* The equality  $\mathcal{L}_{\text{Lyap}} = 0$  implies

$$(\|\mathbf{z}_{t+1}\|_P^2 - \|\mathbf{z}_t\|_P^2)_+ = 0 \quad (24)$$

almost surely, and thus

$$\|\mathbf{z}_{t+1}\|_P^2 \leq \|\mathbf{z}_t\|_P^2 \quad (25)$$

for all  $\mathbf{z}_t$  in the support. Using  $\mathbf{z}_{t+1} = \mathcal{K}_\phi \mathbf{z}_t$ ,

$$\mathbf{z}_t^\top \mathcal{K}_\phi^\top P \mathcal{K}_\phi \mathbf{z}_t \leq \mathbf{z}_t^\top P \mathbf{z}_t, \quad (26)$$

or equivalently

$$\mathbf{z}_t^\top (\mathcal{K}_\phi^\top P \mathcal{K}_\phi - P) \mathbf{z}_t \leq 0 \quad (27)$$

for all  $\mathbf{z}_t$  in a set that spans  $\mathbb{R}^d$ . A symmetric matrix  $M$  satisfies  $M \preceq 0$  if and only if  $\mathbf{z}^\top M \mathbf{z} \leq 0$  for all  $\mathbf{z}$ , hence  $\mathcal{K}_\phi^\top P \mathcal{K}_\phi - P \preceq 0$ .  $\blacksquare$

Conversely, classical results in linear systems theory relate such a Lyapunov inequality to spectral stability.

*Proposition 6 (Spectral stability from a Lyapunov certificate):* Let  $\mathcal{K} \in \mathbb{R}^{d \times d}$  and suppose there exists  $P \succ 0$  such that

$$\mathcal{K}^\top P \mathcal{K} - P \prec 0. \quad (28)$$

Then  $\rho(\mathcal{K}) < 1$ .

*Proof:* Since  $P \succ 0$ , write  $P = R^\top R$  for some invertible  $R \in \mathbb{R}^{d \times d}$  and consider the similarity transform  $\tilde{\mathcal{K}} = R \mathcal{K} R^{-1}$ . The Lyapunov inequality becomes

$$\mathcal{K}^\top P \mathcal{K} - P = \mathcal{K}^\top R^\top R \mathcal{K} - R^\top R = R^\top (\tilde{\mathcal{K}}^\top \tilde{\mathcal{K}} - I) R \prec 0. \quad (29)$$

Premultiplying and postmultiplying by  $(R^{-1})^\top$  and  $R^{-1}$  yields  $\tilde{\mathcal{K}}^\top \tilde{\mathcal{K}} - I \prec 0$ , which implies  $\|\tilde{\mathcal{K}}\mathbf{x}\|_2^2 < \|\mathbf{x}\|_2^2$  for all  $\mathbf{x} \neq 0$ , hence  $\|\tilde{\mathcal{K}}\|_2 < 1$ . Therefore  $\rho(\tilde{\mathcal{K}}) < 1$ , and since  $\mathcal{K}$  and  $\tilde{\mathcal{K}}$  are similar,  $\rho(\mathcal{K}) = \rho(\tilde{\mathcal{K}}) < 1$ .  $\blacksquare$

For finite Lyapunov regularization weight, the penalty  $\mathcal{L}_{\text{Lyap}}$  need not vanish exactly; nevertheless, Propositions 5–6 show that it biases the learned propagator toward the set of operators admitting a Lyapunov certificate of stability, in a way that complements the direct spectral constraints imposed by the ODO parameterization.

Taken together, Propositions 1–6 show that the learnable Koopman family used in Learnable–DeepKoopFormer: (i) provides a clear, tunable stability margin via  $\rho_{\max}$  and the Lyapunov weight; (ii) retains the full expressiveness of spectrally bounded linear dynamics; (iii) admits low-rank specializations capturing dominant latent modes; and (iv) supports well-conditioned inverse propagation when the spectrum is bounded away from zero. These guarantees hold uniformly across all instantiations of Learnable–DeepKoopFormer built on top of the PatchTST, Autoformer, and Informer backbones.

5) *Theoretical stability advantage of the Koopman layer*: We compare the latent dynamics induced by the proposed Koopman layer with those of an unconstrained linear state-space model (SSM). We have shown how all Learnable–DeepKoopFormer variants propagate a latent state  $\mathbf{z}_t \in \mathbb{R}^d$  according to

$$\mathbf{z}_{t+1} = \mathcal{K}_\phi \mathbf{z}_t, \quad (30)$$

where  $\mathcal{K}_\phi$  is parameterised via an orthogonal–diagonal–orthogonal (ODO) factorisation,

$$\mathcal{K}_\phi = U_\phi \text{diag}(\Sigma_\phi) V_\phi^\top. \quad (31)$$

Here  $U_\phi, V_\phi \in \mathbb{R}^{d \times r}$  have orthonormal columns, obtained through QR retraction, and the spectral coefficients  $\Sigma_\phi \in \mathbb{R}^r$  are generated from unconstrained raw parameters  $S$  via a componentwise squashing map

$$\Sigma_{i,\phi}(\theta) = \rho_{\max} \sigma(S_i), \quad \sigma : \mathbb{R} \rightarrow (0, 1), \quad 0 < \rho_{\max} < 1. \quad (32)$$

In contrast, the SSM baseline evolves a hidden state  $h_t \in \mathbb{R}^{d_h}$  as

$$h_{t+1} = Ah_t + Bx_t, \quad \hat{y}_t = Ch_t, \quad (33)$$

where  $A, B, C$  are completely unconstrained. In particular, no analogous spectral and contraction constraints to the ones for  $\mathcal{K}_\phi$  are imposed on the SSM transition matrix  $A$  in (33). In the following Theorem we formally address core stability advantage of the Koopman parameterisation.

*Theorem 1:* Let  $\mathcal{K}_\phi(\rho_{\max})$  denote the class of Koopman operators realised by the ODO-based spectral-squashing parameterisation, such that  $\|\mathcal{K}_\phi\|_2 < \rho_{\max} < 1$  for all  $\mathcal{K}_\phi \in \mathcal{K}_\phi(\rho_{\max})$ . Let  $\mathcal{A}$  denote the class of unconstrained state-space transition matrices. Then: (i) For every  $\mathcal{K}_\phi \in \mathcal{K}_\phi(\rho_{\max})$ , the latent dynamics  $z_{t+1} = \mathcal{K}_\phi z_t$  are uniformly exponentially stable at all training iterates. (ii) The class  $\mathcal{A}$  contains matrices with arbitrarily large spectral radius; moreover, for any finite prediction horizon, there exist unstable  $A \in \mathcal{A}$  that achieve the same finite-horizon training loss as a stable model.

*Proof:*

a) (i) *Stability of the Koopman parameterisation:* By Proposition 1 and Corollary 1, for all  $\mathcal{K}_\phi \in \mathcal{K}_\phi(\rho_{\max})$  the latent dynamics satisfy (see (15))

$$\|z_t\|_2 \leq \rho_{\max}^t \|z_0\|_2, \quad (34)$$

which proves uniform exponential stability.

b) (ii) *Unstable but loss-equivalent SSM solutions:* The unconstrained class  $\mathcal{A}$  contains matrices with arbitrarily large spectral radius: for any  $\gamma > 0$ ,  $A = \gamma I$  satisfies  $\rho(A) = \gamma$ . Now consider a stable SSM  $h_{t+1} = Ah_t + Bx_t$ ,  $\hat{y}_t = Ch_t$  that achieves a given finite-horizon loss over  $t = 0, \dots, H$ . Define an augmented state  $\tilde{h}_t = [h_t^\top, w_t^\top]^\top$  with dynamics

$$\tilde{h}_{t+1} = \begin{bmatrix} A & 0 \\ 0 & \gamma I \end{bmatrix} \tilde{h}_t + \begin{bmatrix} B \\ 0 \end{bmatrix} x_t, \quad \hat{y}_t = [C \ 0] \tilde{h}_t, \quad (35)$$

where  $\gamma > 1$  and  $\tilde{h}_0 = [h_0^\top, 0^\top]^\top$ . Then  $w_t \equiv 0$  for all  $t \leq H$ , so the augmented model produces identical outputs and achieves the same finite-horizon loss, while its transition matrix has spectral radius  $\gamma > 1$ . Choosing  $\gamma$  arbitrarily large completes the proof. ■

6) *Invertibility in finite dimensions and Banach space extension:* Let  $(\mathcal{X}, \|\cdot\|)$  be a Banach space and let  $T : \mathcal{X} \rightarrow \mathcal{X}$  denote the (possibly nonlinear) time-1 evolution map of an underlying dynamical system. The Koopman operator acting on observables  $J : \mathcal{X} \rightarrow \mathbb{R}$  is

$$(\mathcal{K}_\phi J)(x) = J(T(x)), \quad (36)$$

which is linear even if  $T$  is nonlinear. If  $T$  is bijective, then  $\mathcal{K}_\phi$  is invertible with  $\mathcal{K}_\phi^{-1} J = J \circ T^{-1}$ . Thus invertibility of the latent propagator corresponds to bijectivity of the underlying state update. In DeepKoopFormer we learn a *finite-dimensional approximation* of  $\mathcal{K}_\phi$  using an ODO-structured linear operator

$$\mathcal{K}_\phi = U_\phi \text{diag}(\Sigma_\phi) V_\phi^\top, \quad U_\phi, V_\phi \in O(d), \quad \Sigma_i \in (0, \rho_{\max}).$$

Because  $0 < \Sigma_{i,\phi} < \rho_{\max} < 1$ , the operator  $\mathcal{K}_\phi$  is invertible and belongs to the general linear group

$$GL(d) := \{M \in \mathbb{R}^{d \times d} \mid \det(M) \neq 0\},$$

that is, the group of all invertible  $d \times d$  real matrices. Its inverse is given by

$$\mathcal{K}_\phi^{-1} = V_\phi \text{diag}(\Sigma_\phi^{-1}) U_\phi^\top,$$

with operator norm bounds  $\|\mathcal{K}_\phi\|_2 \leq \rho_{\max}$  and  $\|\mathcal{K}_\phi^{-1}\|_2 \leq 1/\sigma_{\min}(\mathcal{K}_\phi) < 1/\rho_{\max}$ .

This yields a finite-dimensional surrogate of an invertible discrete-time Koopman evolution operator, for which  $\mathcal{K}_\phi^n \rightarrow 0$  as  $n \rightarrow \infty$  while backward iterates  $\mathcal{K}_\phi^{-n}$  remain well-defined and bounded.

In contrast, standard state-space models with unconstrained transition matrices  $A$  (as commonly used in classical linear SSMs and recent deep state-space architectures) provide no such guarantees:  $A$  may be singular, ill-conditioned, or unstable, and even when invertible its spectral properties are not explicitly controlled [61], [62], [63].

Consequently, the Koopman propagator used in Learnable-DeepKoopFormer yields a stable, invertible, finite-dimensional representation of latent dynamics, whereas unconstrained SSM formulations lack explicit spectral and stability guarantees.

#### IV. NUMERICAL SIMULATIONS

To evaluate the proposed Learnable-DeepKoopFormer architecture in a controlled yet systematically scalable setting, we employ a unified Koopformer benchmark pipeline on multivariate real-valued time series. From each dataset we construct sliding windows of length  $P$  and corresponding forecast targets of length  $H$ , using a grid of input-output configurations with  $P \in \{80, 100, 120, 140\}$  and  $H \in \{4, 8, 12, 16\}$ . The windows are normalised feature-wise and split into training and test sets using an 80%/20% chronological partition.

a) *Model hyperparameters:* To ensure a fair comparison, we keep the capacity of all architectures fixed across experiments. For both PatchTST and Informer, the Transformer encoder uses  $L = 3$  layers with hidden dimension  $d_{\text{model}} = 96$ ,  $h = 4$  attention heads, and feed-forward width  $d_{\text{ff}} = 96$ . The Autoformer backbone employs the same number of layers and heads with  $d_{\text{model}} = 96$  and a slightly narrower feed-forward width  $d_{\text{ff}} = 64$ . In all cases, the patch size (for PatchTST and Informer) and the moving-average window (for Autoformer) are tied to the input window length  $P$ , and token-level representations are pooled into a single latent vector.

The Koopman layer in the constrained and learnable regimes acts on a latent state of dimension  $d_{\text{lat}} = d_{\text{model}}$  for PatchTST and Informer, and  $d_{\text{lat}} = H$  for Autoformer. The strictly stable and learnable variants enforce an upper bound  $\rho(\mathcal{K}_\phi) < \rho_{\max}$  with  $\rho_{\max} = 0.99$ , whereas the unconstrained variant uses a free dense matrix in  $\mathbb{R}^{d_{\text{lat}} \times d_{\text{lat}}}$ . Within the Learnable-DeepKoopFormer family, the scalar-gated and per-mode gated operators use global and dimension-wise  $(\alpha, \beta)$  parameters, respectively; MLP-shaped spectral mapping employs a one-hidden-layer MLP to parameterise the spectrum; and the low-rank Koopman variant uses rank  $r = 16$ , i.e.  $\mathcal{K}_\phi = U_{r,\phi} \text{diag}(\Sigma_{r,\phi}) V_{r,\phi}^\top$  with  $U_r, V_r \in \mathbb{R}^{d_{\text{lat}} \times 16}$ .

For the non-Koopman baselines, the LSTM forecaster uses  $L = 2$  recurrent layers with hidden size 96, the DLinear model implements a single shared linear map from the length- $P$  history of each channel to the  $H$ -step forecast, and the discrete-time state-space model uses a latent state of dimension 96 with a linear readout to  $\mathbb{R}^{H \cdot d}$ . All models are trained with the Adam optimizer (learning rate  $3 \times 10^{-4}$ ) for 4,000 gradient steps per  $(P, H)$  configuration; the Lyapunov regularisation weight is set to  $\lambda_{\text{Lyap}} = 0.1$  for constrained, learnable, and unconstrained Koopman variants unless stated otherwise.

*b) Spectral logging and diagnostics:* For all models with an explicit linear propagator, we record spectral quantities that describe stability and latent energy dynamics. In Koopman-based architectures, the update  $z_{t+1} = \mathcal{K}_\phi z_t$  is controlled by the spectrum of the learned transition matrix  $\mathcal{K}_\phi$ , which determines how latent signals contract or amplify over time.

In the constrained and learnable ODO variants, the transition operator is written in factorised form  $\mathcal{K}_\phi = U_\phi \Sigma_\phi V_\phi^\top$ , where  $U_\phi$  and  $V_\phi$  are orthonormal and  $\Sigma_\phi = \text{diag}(\sigma_{i,\phi})$  is produced by a squashing map restricting each  $\sigma_{i,\phi}$  to  $(0, \rho_{\max})$  with  $\rho_{\max} < 1$ . We therefore log the singular values  $\{\sigma_i(\mathcal{K}_\phi)\}$  and in particular track  $\max_i \sigma_i(\mathcal{K}_\phi)$  as a proxy for the spectral radius. This provides a direct view of how different parametrisations (scalar, per{mode, MLP{based, low{rank}) populate the disc of radius  $\rho_{\max}$ .

To disentangle the effect of spectral structure in the latent dynamics, we evaluate three linear-transition regimes: *constrained Koopman* (constr), *unconstrained Koopman* (unconstr), and a standard *linear state-space model (SSM)* baseline. In the constrained regime, the latent propagator is parameterized via an orthogonal-diagonal-orthogonal (ODO) factorization,  $\mathcal{K}_\phi = U_\phi \text{diag}(\Sigma_\phi) V_\phi^\top$ , where the spectral coefficients are squashed to satisfy  $\max_i |\Sigma_{\phi,i}| < \rho_{\max} < 1$ , ensuring a uniform contraction bound and stable latent rollouts. In the unconstrained Koopman regime, we retain the same encoder-propagator-decoder pipeline but replace the ODO structure with a free dense matrix  $\mathcal{K}_\phi \in \mathbb{R}^{d \times d}$ , learned directly from data without explicit spectral-radius constraints; this variant maximizes linear expressiveness but may admit unstable or poorly conditioned transitions, hence we monitor its eigen-spectrum  $\{\lambda_i(K_\phi)\}$  and spectral radius  $\rho(\mathcal{K}_\phi) = \max_i |\lambda_i(\mathcal{K}_\phi)|$  during training. As a non-Koopman baseline, we consider a discrete-time linear SSM of the form  $h_{t+1} = Ah_t + Bx_t$  with prediction  $\hat{y}_t = Ch_t$ , where the transition matrix  $A$  is likewise learned without explicit spectral control. Because  $A$  is generally non-normal, transient growth is governed by the operator norm rather than eigenvalues; accordingly, we log its singular values (in particular the maximum singular value of  $A$ ) as a stability/conditioning diagnostic. Together, these three regimes provide a controlled comparison between (i) explicitly spectrally shaped latent dynamics (constrained Koopman), (ii) fully free linear latent dynamics within the Koopman pipeline (unconstrained Koopman), and (iii) classical unconstrained linear state-space evolution (SSM).

Overall, this spectral logging procedure converts each trained model into a spectral data point, enabling distributional comparisons (e.g., violin plots) that expose stability-accuracy

trade-offs across Koopman parametrisations and backbones.

*c) Benchmark Datasets:* To evaluate the forecasting performance of Learnable-DeepKoopFormer we investigate three heterogeneous and dynamically rich real-world domains: *climate systems*, *financial markets*, and *electricity generation*. These domains exhibit nonstationarity, multiscale temporal dependencies, and nonlinear interactions—conditions under which classical deep forecasting models often face difficulties.

For climate analysis and renewable energy applications, we employ atmospheric data from CMIP6<sup>5</sup> and ERA5<sup>6</sup>, capturing regional wind speed and surface pressure over Germany [64], [65], [8]. As a complementary nonlinear system, we analyze cryptocurrency market behavior using a publicly available multivariate dataset<sup>7</sup>, which includes volatility, pricing trends, and trading activity for major digital assets—an archetypal example of stochastic, regime-switching dynamics. Finally, we examine trends in national energy production by modeling electricity generation in Spain<sup>8</sup> across fossil, wind, solar, hydro, and biomass sources, where physical constraints and weather dependencies induce complex temporal couplings. Together, these datasets span distinct dynamical regimes and provide a rigorous foundation for assessing the ability of Koopman-enhanced representations to extract latent linear structure from nonlinear temporal processes.

*d) Hardware Configuration:* All experiments were executed on a high-performance computing (HPC) system with dual AMD EPYC 9554 processors (128 cores per node, multithreaded) and 1.5 TB shared memory, suitable for large context windows and attention-based models. Training was accelerated using NVIDIA L40S GPUs supporting mixed-precision tensor operations. Resource allocation and job scheduling were managed through the Slurm workload manager with exclusive node access to ensure reproducible performance.

*e) Code availability statement:* The Learnable-DeepKoopFormer framework—including source code, datasets, and representative figures—is accessible at Github<sup>9</sup> and Zenodo<sup>10</sup>. The entire implementation is written in Python and builds upon standard scientific computing libraries, including PyTorch, NumPy, and SciPy.

### A. Discussion on Wind Speed dataset

For the CMIP6-based wind-speed forecasting task, Fig. 1 depicts the distributions of train/test MSE and MAE across all patch-length and horizon configurations. The Koopman-enhanced Transformers (PatchTST, Autoformer, Informer) exhibit *tightly concentrated, low-centred* violins

<sup>5</sup><https://cds.climate.copernicus.eu/datasets/projections-cordex-domains-single-levels?tab=overview>

<sup>6</sup><https://cds.climate.copernicus.eu/datasets>

<sup>7</sup><https://github.com/Chisomnwa/Cryptocurrency-Data-Analysis>

<sup>8</sup><https://github.com/afshinfaramarzi/Energy-Demand-electricity-price-Forecasting/tree/main>

<sup>9</sup><https://github.com/Ali-Forootani/Learnable-DeepKoopFormer>

<sup>10</sup><https://doi.org/10.5281/zenodo.17988424>, <https://doi.org/10.5281/zenodo.18115612>

in all four panels, indicating consistently low errors and a remarkable stability across forecasting conditions. In contrast, the recurrent and linear baselines (LSTM, DLinear, SSM) display *higher-centred* distributions with visibly broader shapes, reflecting larger error levels and increased sensitivity to patch length and horizon changes. Within the Koopman family, the `constr` variant shows the most compact and low-error violins, particularly for PatchTST, highlighting the effect of spectral constraints on stabilising latent dynamics. The learnable variants (scalar-gated, per-mode gated, MLP-shaped spectral mapping, low-rank Koopman) maintain similarly low medians with slightly wider spreads, suggesting a trade-off between expressive dynamics and variability. The `unconstr` operator produces noticeably broader tails—especially in the PatchTST backbone—which implies that removing spectral control can reduce robustness, even though median errors remain competitive.

Overall, based on violin distributions alone, Koopman–Transformer models are not only more accurate than recurrent or linear baselines, but also substantially more stable across a wide range of forecasting configurations.

*a) Koopman spectra across backbones - Wind Speed:* For each trained configuration (choice of patch length and forecast horizon), we extract the spectrum of the latent transition operator and pool all spectral magnitudes  $\rho = |\lambda|$  at the level of Autoformer, Informer, and PatchTST backbones and their Koopman variants. Figure 2 reports these pooled distributions as violins, together with the singular-value spectrum of the SSM baseline. Across all backbones, the strictly stable Koopman variants (“`constr`”) exhibit compact spectra: the bulk of the mass lies between approximately  $\rho \approx 0.3$  and  $\rho \approx 0.8$ , with essentially no values above 1, confirming that the spectral-radius constraint is respected in practice. The learnable families (scalar-gated, per-mode gated, MLP-shaped spectral mapping, low-rank Koopman) occupy a similar central range but display visibly broader violins and slightly heavier upper tails, indicating that these parametrisations exploit a larger portion of the admissible disc while still remaining predominantly contractive. In contrast, the unconstrained Koopman variants (“`unconstr`”) concentrate their spectra very close to the origin, with most magnitudes below  $\rho \approx 0.2$ , which reflects the combined effect of data fitting and the Lyapunov regularisation term driving the latent dynamics towards strongly damped behaviour. The SSM baseline forms a narrow distribution at small spectral magnitudes (around  $\rho \approx 0.05$ – $0.2$ ) with a thin tail extending towards and *beyond the unit circle*, consistent with occasional large singular values of the state-transition matrix in an unconstrained linear state-space model. Overall, the figure shows that the dominant differences in spectral behaviour are induced by the Koopman parameterisation (constrained vs. learnable vs. unconstrained) rather than by the specific Transformer backbone, and that the Koopman-enhanced models achieve expressive yet predominantly stable latent linear dynamics.

#### B. Discussion on Pressure Surface dataset

For the CMIP6-based pressure–surface forecasting task, Fig. 3 summarises the error distributions over all patch–length

and horizon combinations via violin plots of train/test MSE and MAE. Across the four violin panels, the Koopman–Transformer families (PatchTST, Autoformer, Informer) concentrate most of their mass in the lower part of the error axis, with visibly tight and compact distributions. In contrast, the purely recurrent and linear baselines (LSTM, DLinear, SSM) exhibit higher-centred violins with noticeably wider spread in several cases. Within the Koopman–enhanced models, the constrained operator (`constr`) yields the most compact and low-variance distributions across all backbones. The learnable operator families (scalar-gated, per-mode gated, MLP-shaped spectral mapping, low-rank Koopman) produce slightly broader violins, reflecting increased expressive capacity with a small variability trade-off. By contrast, the unconstrained operator (`unconstr`) exhibits heavier tails—especially for PatchTST and Informer—even when its median error remains competitive, indicating reduced robustness when no spectral regularisation is enforced. A notable exception emerges in the test–set summary: while Koopman variants remain among the most stable across patch lengths and horizons, *certain baseline configurations* (particularly DLinear and SSM) achieve *slightly lower mean test errors* for the pressure–surface task. However, these gains are offset by substantially wider violin spreads, indicating less predictable generalisation across forecasting conditions. In contrast, the Koopman family achieves comparable or near-best means with significantly reduced spread, suggesting a more stable latent dynamics model that balances expressive power and robustness rather than relying on chance favourable configurations.

*a) Koopman spectra across backbones - Pressure Surface:* For each trained configuration on the pressure–surface data, we extract all latent spectral magnitudes  $\rho = |\lambda|$  and pool them by backbone and Koopman variant. Figure 4 shows the resulting distributions. Across Autoformer, Informer, and PatchTST, the constrained variants (`constr`) concentrate their spectra in a compact band  $\rho \approx 0.3$ – $0.8$ , with no values exceeding 1, indicating that the spectral-radius constraint is enforced in practice. The learnable variants (scalar-gated, per-mode gated, MLP-shaped spectral mapping, low-rank Koopman) occupy a similar range but with broader distributions and mildly heavier tails, reflecting increased expressive capacity while remaining largely contractive. The unconstrained variants (`unconstr`) collapse toward strongly damped dynamics, with most magnitudes below  $\rho \approx 0.2$ . The SSM baseline likewise concentrates at small values but exhibits a thin upper tail extending towards and *occasionally above the unit circle*. Overall, differences in spectral behavior arise predominantly from the Koopman parameterisation rather than from the choice of Transformer backbone, and Koopman–enhanced models realise stable latent dynamics for large–scale pressure–surface forecasting.

#### C. Discussion on Cryptocurrency dataset

For the cryptocurrency forecasting task, Fig. 5 reports the distribution of train/test MSE and MAE across all patch–length and horizon configurations using violin plots. The Koopman–Transformer families (PatchTST,

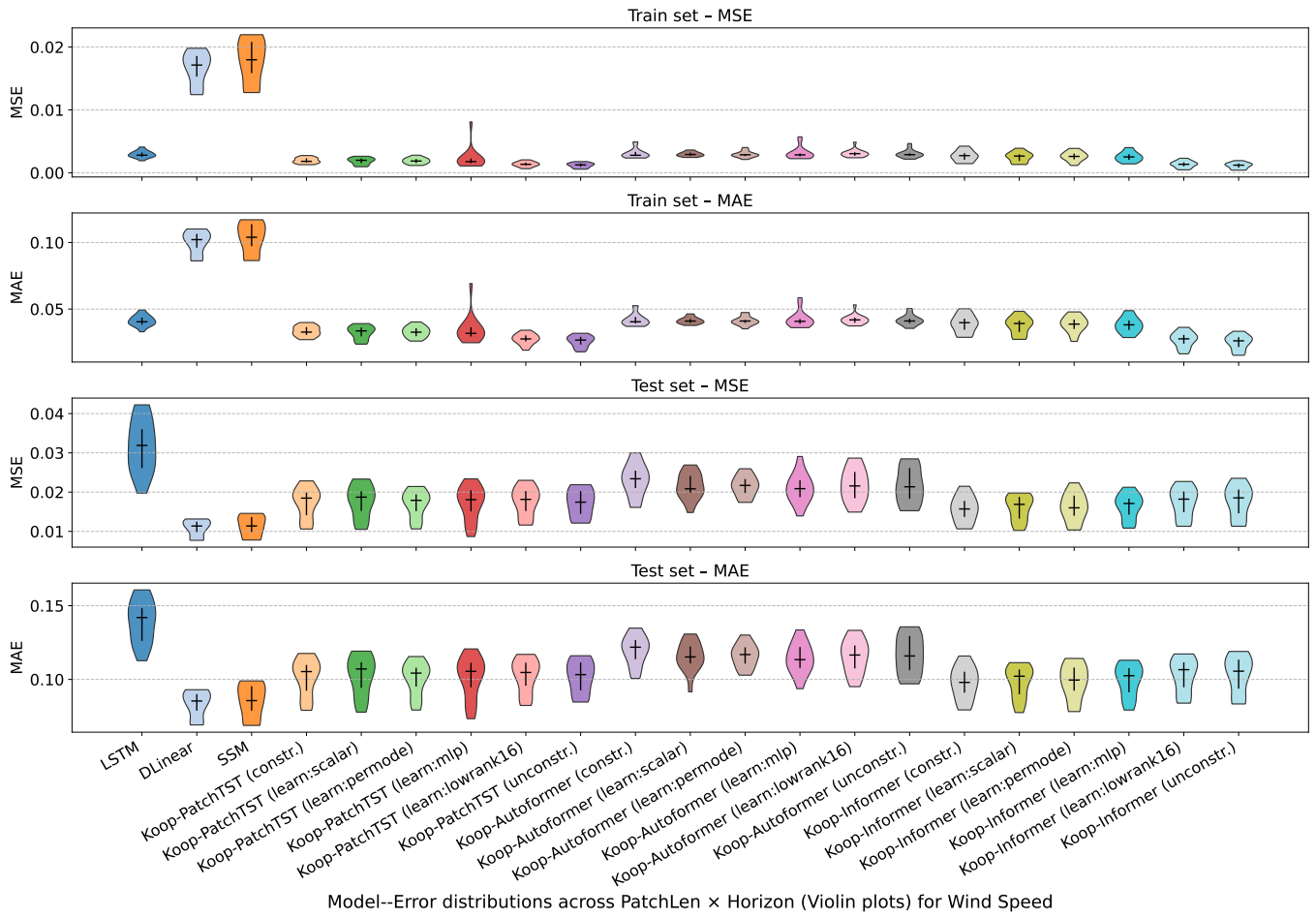


Fig. 1: Violin plots of train/test MSE and MAE for all architectures on the wind speed forecasting task, aggregated over all patch lengths and horizons.

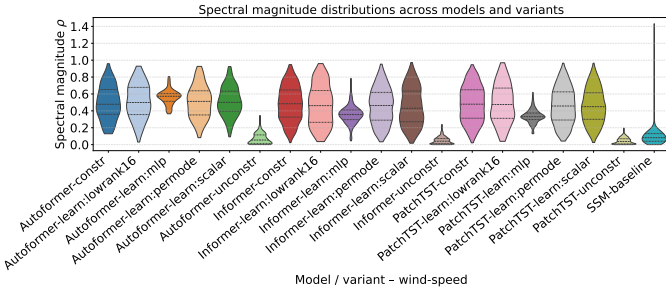


Fig. 2: Spectral distributions of latent Koopman operators for CIMIP6 wind speed forecasting task.

Autoformer, Informer) generally form compact, low-centred distributions, indicating stable forecasting behaviour across hyperparameter choices. In contrast, the recurrent and linear baselines (LSTM, DLinear, SSM) display visibly broader spreads and higher variability, suggesting more sensitive performance to architectural and hyperparameter changes. Among Koopman variants, the constrained operator (constr) achieves the most concentrated error distributions on both training and test sets, highlighting the benefits of explicit spectral stabilisation in highly fluctuating crypto time series.

Learnable operator families (scalar-gated, per-mode gated, MLP-shaped spectral mapping, low-rank Koopman) obtain competitive or near-best median errors, albeit with slightly wider spreads that reflect the trade-off between flexibility and stability. By contrast, the unconstrained operator (unconstr) exhibits heavier tails for PatchTST and Informer, despite a competitive median value, illustrating reduced robustness when no spectral control is imposed.

a) *Koopman spectra across backbones — Cryptocurrency*: For the cryptocurrency forecasting experiments, we collect all latent spectral magnitudes  $\rho = |\lambda|$  from the trained models and group them by backbone and Koopman variant. Figure 6 displays the resulting distributions across PatchTST, Autoformer, and Informer. Across all three backbones, the constrained Koopman operator (constr) yields compact spectra centred around  $\rho \approx 0.3\text{--}0.6$ , with no values approaching the unit circle. This consistent boundedness indicates that the spectral constraint is effectively enforced, promoting stable latent evolution even under the pronounced volatility of crypto price dynamics. The learnable operator families (scalar-gated, per-mode gated, MLP-shaped spectral mapping, low-rank Koopman) occupy similar or slightly wider ranges, typically  $\rho \approx 0.3\text{--}0.8$ , and exhibit moderately heavier tails. This reflects their in-

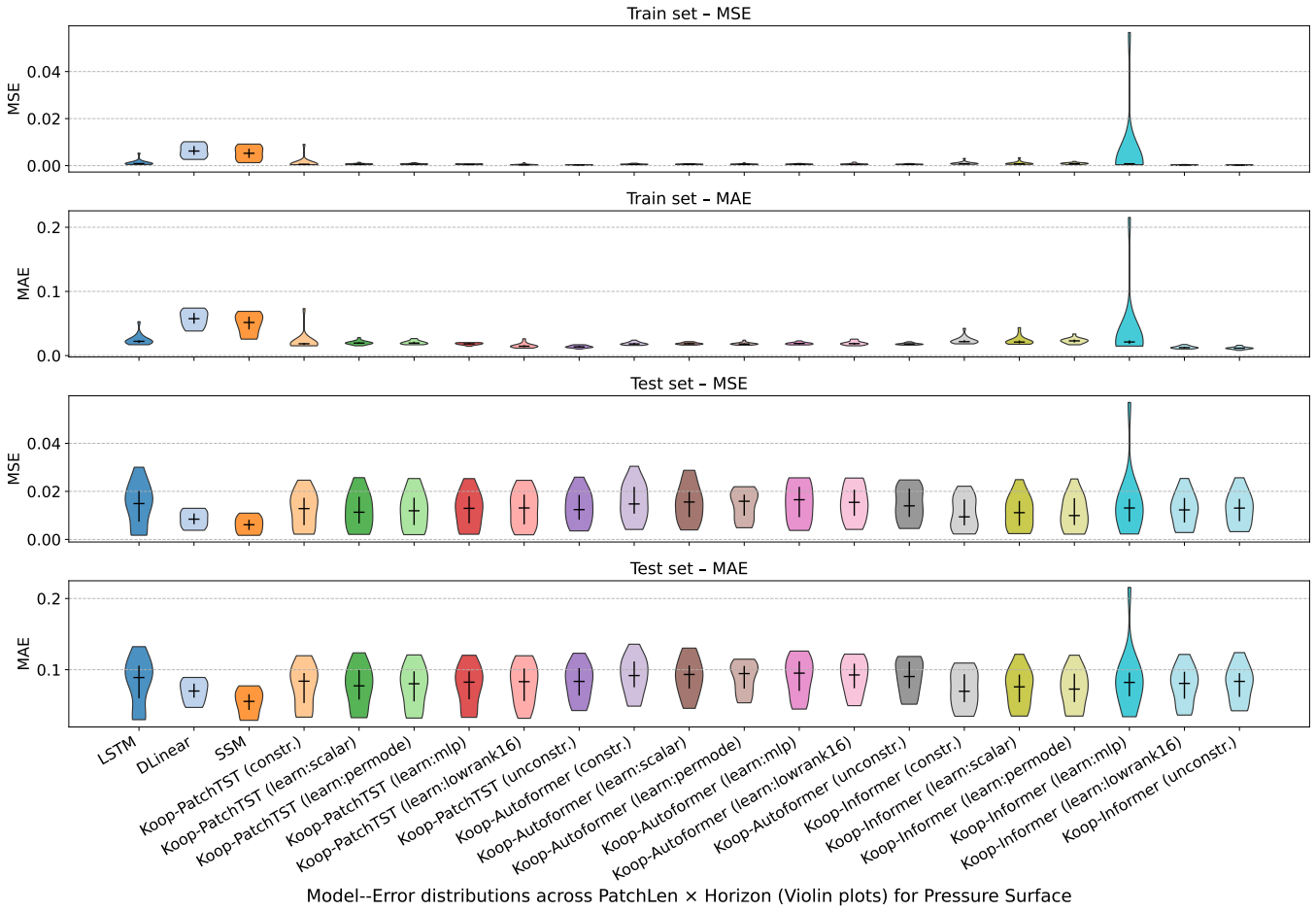


Fig. 3: Violin plots of train/test MSE and MAE for all architectures on the pressure surface forecasting task, aggregated over all patch lengths and horizons.

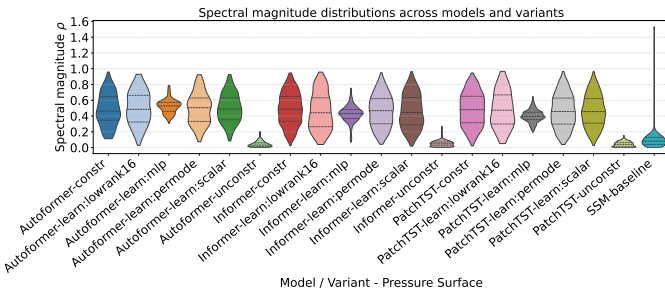


Fig. 4: Spectral distributions of latent Koopman operators for CIMIP6 pressure surface forecasting task.

creased expressive capacity: they can adaptively shape latent temporal scales while remaining largely contractive in practice. In contrast, the unconstrained variant (unconstr) collapses toward strongly damped spectra with  $\rho < 0.2$ , producing overly dissipative latent dynamics. Meanwhile, the SSM baseline concentrates at small magnitudes but shows a distinct thin tail extending toward and beyond  $\rho \approx 1.0$ , indicating occasional unstable latent modes in the absence of explicit spectral control.

#### D. Discussion on Energy Systems Dataset

Figure 7 shows the distribution of train/test MSE and MAE over all patch-length and horizon settings for the energy systems task. Unlike the previous domains, the Autoformer backbone performs noticeably worse: both its baseline and Koopman variants produce high-centred violins with broad tails, indicating weaker forecasting accuracy and a strong sensitivity to hyperparameter choices. The LSTM baseline achieves very low training errors with compact violins, showing strong short-term adaptability. However, its test errors spread widely, revealing limited generalisation and a tendency to overfit. Similarly, DLinear and SSM occasionally attain competitive medians but exhibit inconsistent spreads across configurations, suggesting dependence on specific window and horizon settings rather than robust behaviour. Across all backbones, Koopman-enhanced variants yield more reliable performance. In particular, the constrained operator (constr) consistently produces tight, mid-centred violins with comparatively low variability. While not always the best in terms of median error, it is the most stable across hyperparameters, highlighting the benefit of enforcing spectral bounds in the latent dynamics for slow-varying energy system trends. Learnable operators (scalar-gated, per-mode gated, MLP-shaped

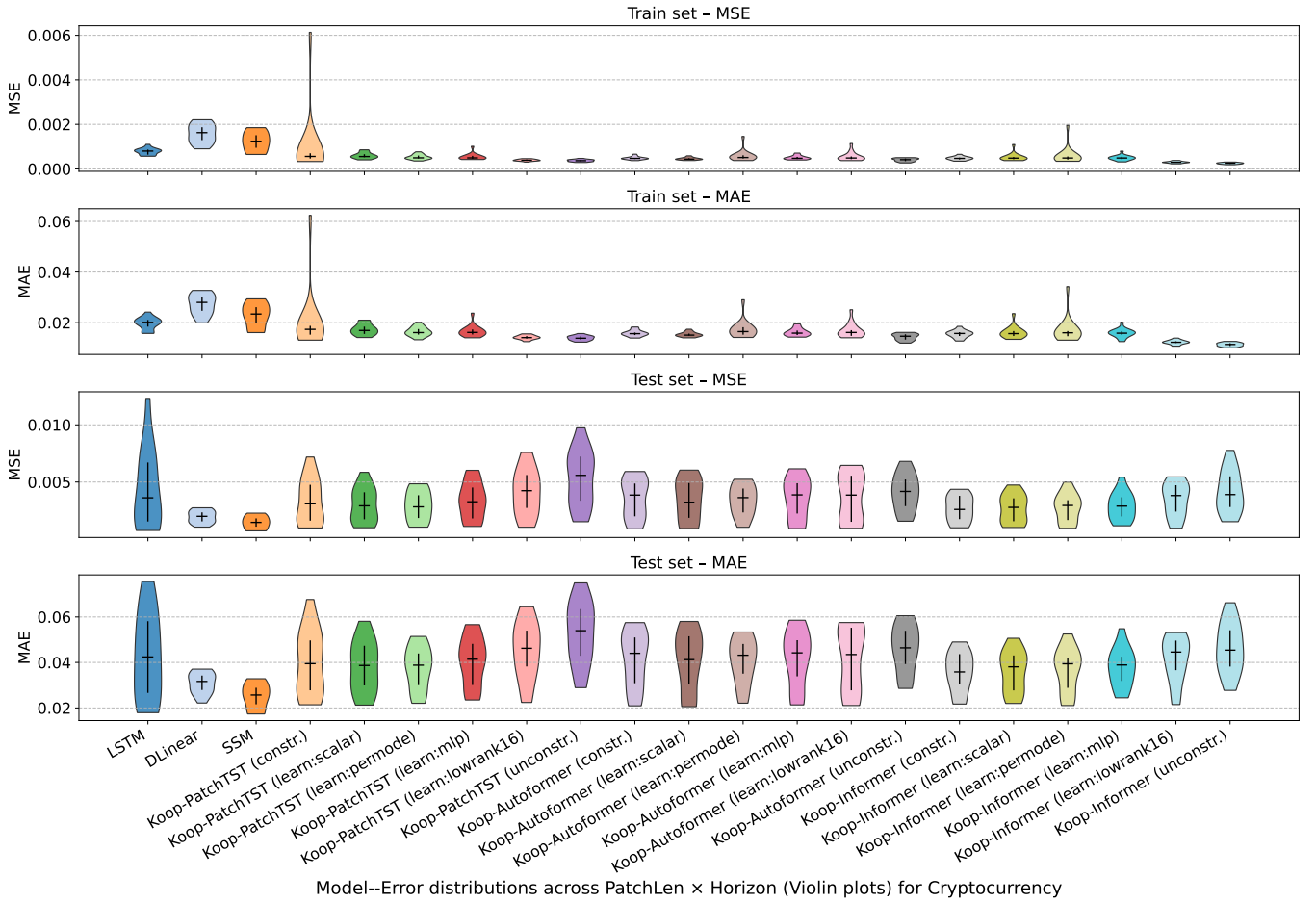


Fig. 5: Violin plots of train/test MSE and MAE for all architectures on the Cryptocurrency forecasting task, aggregated over all patch lengths and horizons.

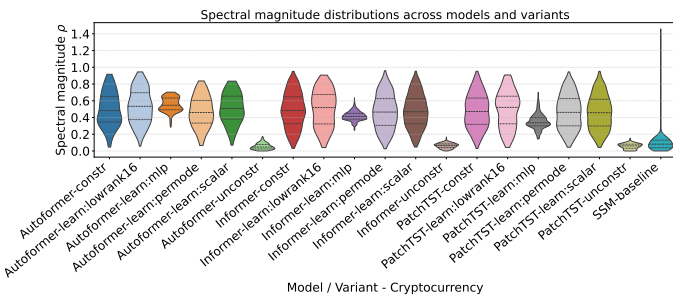


Fig. 6: Spectral distributions of latent Koopman operators for the Cryptocurrency forecasting task.

spectral mapping, low-rank Koopman) achieve competitive medians with slightly broader spreads, reflecting a trade-off between expressiveness and robustness. Overall, the energy systems results demonstrate that minimising training error alone (e.g., LSTM or Autoformer) does not guarantee reliable forecasting. Koopman-enhanced models, particularly with spectral constraints, prioritise stable generalisation across hyperparameter choices, making them well suited for forecasting tasks governed by long-range temporal structure.

*a) Koopman spectra across backbones — Energy Systems:* Figure 8 shows latent spectral magnitudes  $\rho = |\lambda|$  for all model variants in a single violin plot. The constrained Koopman operator (constr) consistently produces compact spectra around  $\rho \approx 0.3\text{--}0.6$ , clearly away from  $\rho = 1$ , indicating stable latent evolution suitable for slowly varying energy trends. The learnable operator families (scalar-gated, per-mode gated, MLP-shaped spectral mapping, low-rank Koopman) span slightly wider ranges ( $\rho \approx 0.3\text{--}0.8$ ), reflecting greater flexibility while remaining largely contractive. In contrast, the unconstrained variant (unconstr) collapses toward very small radii ( $\rho < 0.2$ ), implying overly damped dynamics, whereas the SSM baseline shows predominantly small values with a thin tail beyond  $\rho \geq 1$ , revealing occasional unstable modes. Overall, explicit spectral control enables stable temporal modelling in energy systems data.

#### E. Discussion on ERA5 Wind Speed Dataset

Figure 9 reports train/test error distributions for ERA5 wind forecasting across all patch-length and horizon settings. While most methods reach low medians due to smooth wind dynamics, their robustness differs substantially. LSTM, DLinear, and SSM produce competitive medians but wider

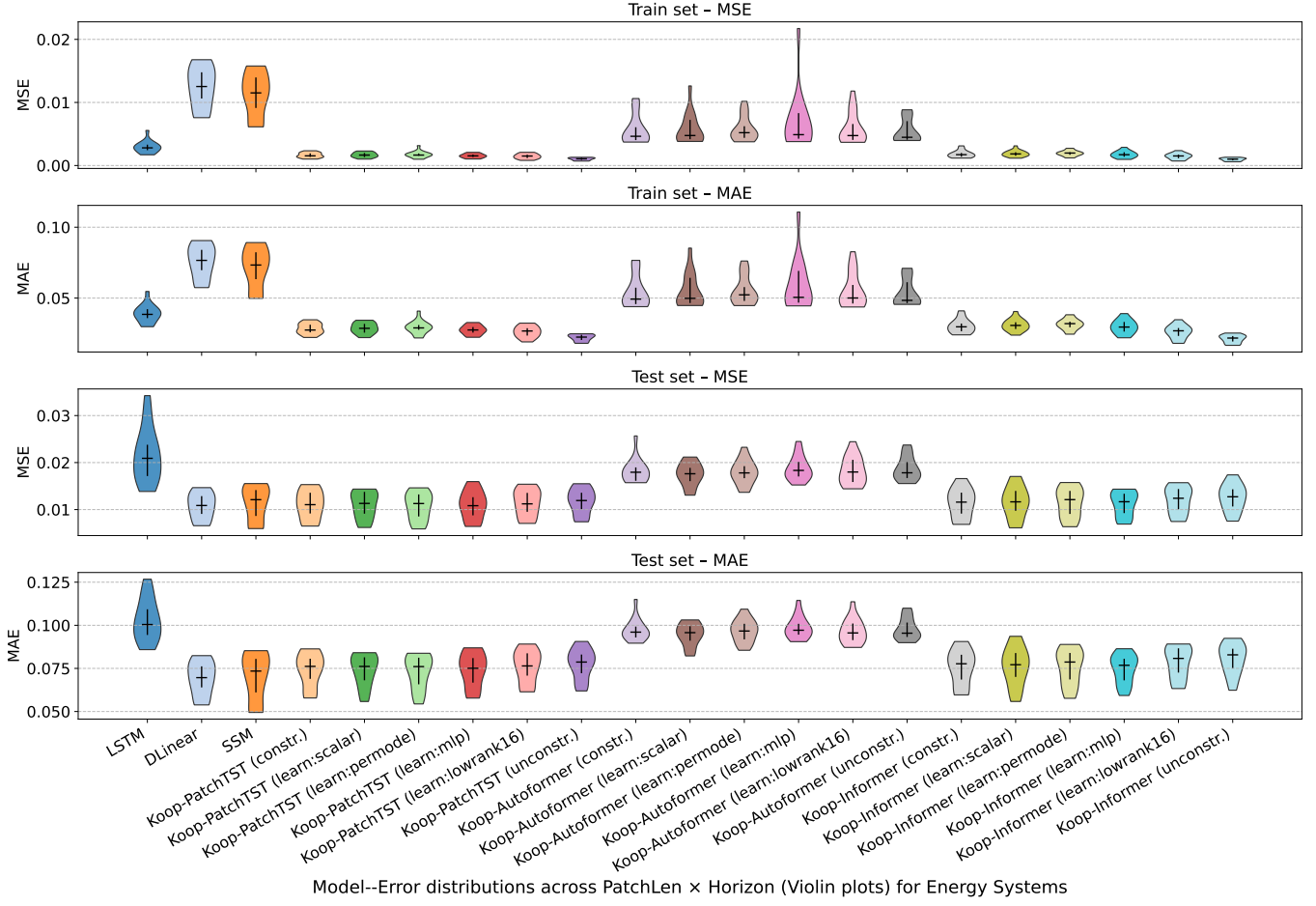


Fig. 7: Violin plots of train/test MSE and MAE for all architectures on the energy systems forecasting task, aggregated over all patch lengths and horizons.

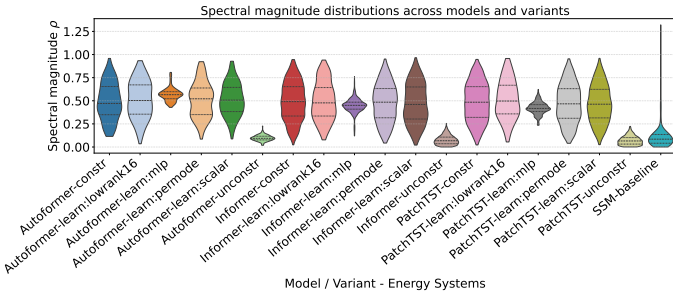


Fig. 8: Spectral distributions of latent Koopman operators for the energy systems forecasting task.

distributions, with LSTM displaying compact training violins yet broader test spreads, indicating mild overfitting. DLinear and SSM fluctuate strongly across settings, limiting reliability. By contrast, Koopman-enhanced models form consistently tight, low-centred violins. The constrained operator (constr) exhibits the most compact train/test distributions, demonstrating stable latent dynamics. Learnable variants (scalar-gated, per-mode gated, MLP-shaped spectral mapping, low-rank Koopman) achieve similar medians with slightly broader spreads, balancing adaptivity and

spectral stability.

*a) Koopman spectra across backbones - ERA5 Wind Speed:* Figure 10 shows latent spectral magnitudes  $\rho = |\lambda|$  for all model variants in a single violin plot. The constrained Koopman operator (constr) consistently produces compact spectra around  $\rho \approx 0.3\text{--}0.6$ , clearly away from  $\rho = 1$ , indicating stable latent evolution suitable for slowly varying energy trends. The learnable operator families (scalar-gated, per-mode gated, MLP-shaped spectral mapping, low-rank Koopman) span slightly wider ranges ( $\rho \approx 0.3\text{--}0.8$ ), reflecting greater flexibility while remaining largely contractive. In contrast, the unconstrained variant (unconstr) collapses toward very small radii ( $\rho < 0.2$ ), implying overly damped dynamics, whereas the SSM baseline shows predominantly small values with a thin tail beyond  $\rho \geq 1$ , revealing occasional unstable modes. Overall, explicit spectral control enables stable temporal modelling in energy systems data.

#### F. Advantages of Learnable-DeepKoopFormer Modules.

The spectral analysis highlights a key benefit of the proposed learnable Koopman modules: they adapt the latent time scales without sacrificing stable and reversible dynamics.

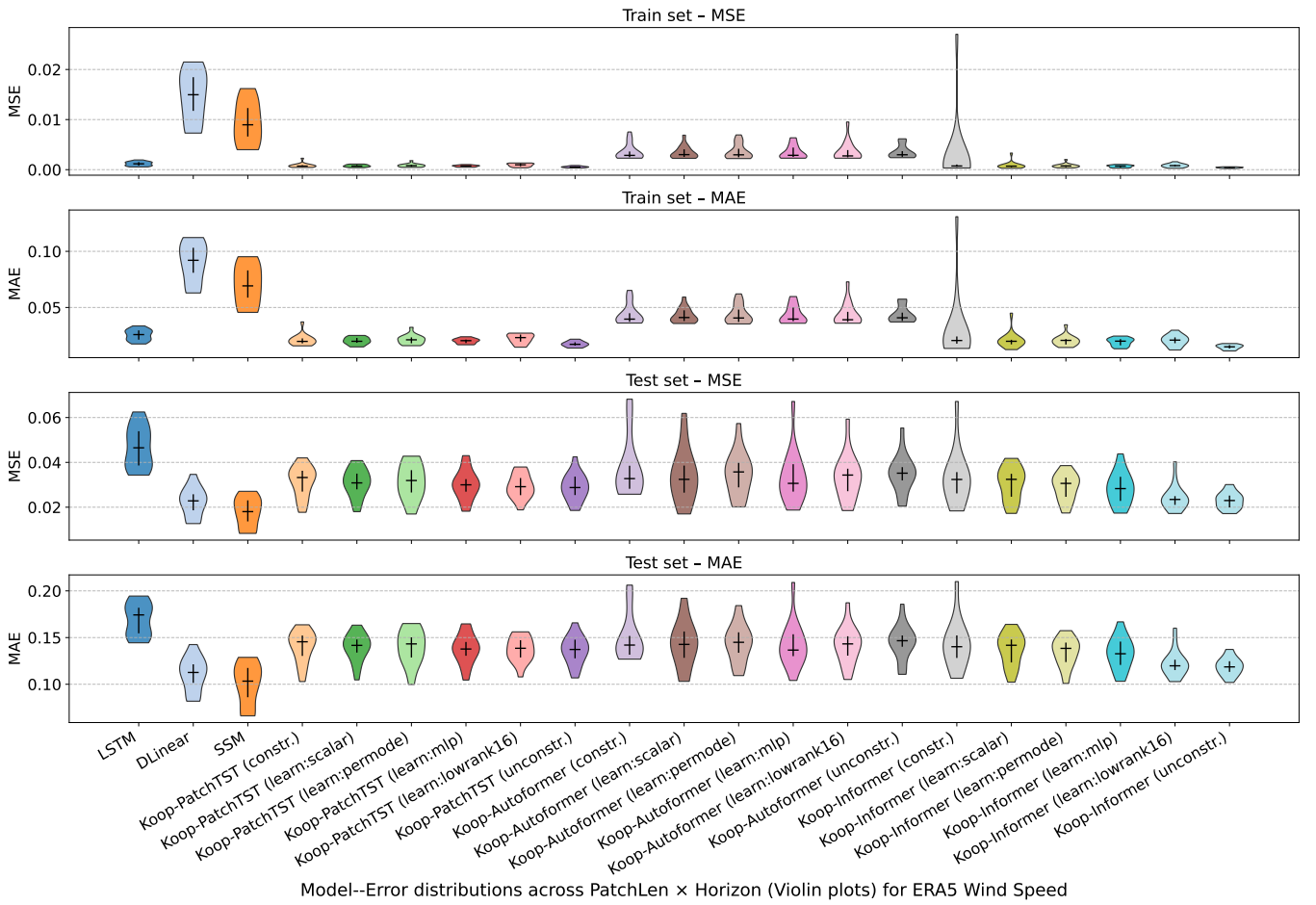


Fig. 9: Violin plots of train/test MSE and MAE for all architectures on the ERA5 wind speed forecasting task, aggregated over all patch lengths and horizons.

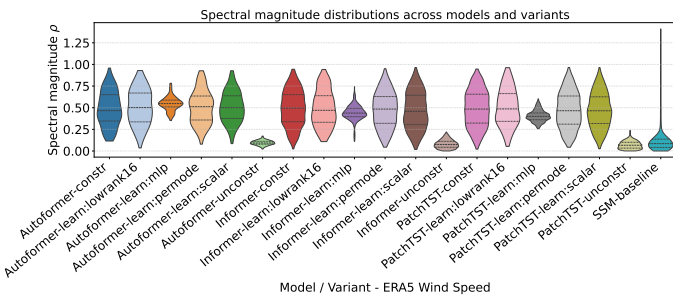


Fig. 10: Spectral distributions of latent Koopman operators for ERA5 wind speed forecasting task.

Whereas purely constrained variants tightly restrict the spectrum, and unconstrained models tend to collapse into strongly damped states ( $|\lambda| \rightarrow 0$ ), the learnable families populate a non-collapsed but contractive range ( $0.3 \lesssim |\lambda| \lesssim 0.8$ ). This region provides enough variability to capture both fast and slow temporal modes, while keeping the spectral radius below unity so that the latent dynamics remain stable. Crucially, because eigenvalues do not decay toward zero, the resulting operators are *invertible*, enabling well-posed backward propagation and preventing information loss over long-range iterative forecasts.

Thus, learnability does not merely increase flexibility; it yields *invertible and non-degenerate latent dynamics*, offering richer temporal structure than constrained models and more reliable long-horizon behaviour than unstable or over-damped baselines.

## V. CONCLUSION

This paper introduced the Learnable-DeepKoopFormer framework, which augments lightweight and full Transformer forecasters with a family of spectrally controlled, learnable Koopman operators. Building on an orthogonal-diagonal-orthogonal (ODO) factorisation, we proposed scalar-gated, per-mode, MLP-shaped, and low-rank Koopman variants that interpolate between strictly constrained and fully unconstrained linear latent dynamics while preserving explicit control over spectrum, stability, and rank. We provided a unified training objective combining standard forecasting loss with Lyapunov-style regularisation, and established theoretical guarantees on spectral stability, contractivity, low-rank structure, and invertibility of the resulting propagators. Together, these results show that Koopman layers can be integrated into modern attention-based backbones in a way that is both

mathematically principled and practically compatible with large-scale time-series forecasting.

Extensive experiments across five heterogeneous real-world datasets—CMIP6 and ERA5 wind speed, CMIP6 surface pressure, cryptocurrency markets, and national-scale electricity generation—demonstrate that Koopman-enhanced Transformers achieve robust and accurate forecasting over a wide grid of input–output configurations. Across all domains, the Koopman variants embedded in `PatchTST`, `Autoformer`, and `Informer` generally yield lower and more tightly concentrated train/test error distributions than recurrent (LSTM) and linear (`DLinear`, `SSM`) baselines, indicating reduced sensitivity to patch length and horizon choices. Constrained Koopman operators systematically provide the most compact error violins and the most stable generalisation behaviour, while the learnable families (scalar-gated, per-mode gated, MLP-shaped spectral mapping, low-rank Koopman) attain comparable or near-best median errors with modestly increased spread, reflecting a favourable trade-off between expressiveness and robustness. Unconstrained operators can match median accuracy but exhibit heavier tails, underscoring that the absence of spectral control tends to degrade reliability rather than improve it.

The spectral diagnostics further clarify the role of the Koopman layer in shaping latent dynamics. Constrained variants consistently populate a mid-range contractive band ( $0.3 \lesssim |\lambda| \lesssim 0.8$ ), ensuring non-explosive but non-collapsed evolution. Learnable variants occupy a similar range with slightly broader support, indicating that they exploit the admissible stability region to adjust latent time scales while remaining predominantly contractive. In contrast, unconstrained Koopman maps often collapse toward very small radii (over-damped dynamics), whereas the `SSM` baseline exhibits thin but non-negligible tails beyond the unit circle, confirming that unrestricted state-space models can drift into spectrally unstable regimes despite good finite-horizon fit. Overall, the spectral analysis shows that the primary differences in latent behaviour are induced by the Koopman parametrisation rather than by the particular Transformer backbone, and that `Learnable-DeepKoopFormer` achieves stable, interpretable, and invertible latent dynamics across diverse dynamical regimes.

From a modelling perspective, the learnable Koopman modules offer a key structural advantage: they adapt latent temporal scales *without sacrificing stability or invertibility*. By avoiding eigenvalues that cluster near zero or exceed the unit circle, the proposed operators maintain non-degenerate, well-conditioned dynamics that support long-range forecasting without catastrophic decay or uncontrolled growth. This makes `Learnable-DeepKoopFormer` particularly suitable for applications where both predictive accuracy and dynamical interpretability matter, such as climate risk assessment, energy systems planning, and financial stress testing, and suggests that spectral control is a powerful inductive bias for deep sequence models.

Several directions remain open for future work. On the theoretical side, extending the analysis to explicitly stochastic or non-stationary settings, and connecting spectral constraints to distributional robustness and uncertainty quantification, are promising avenues. On the modelling side, integrating control inputs and exogenous covariates into the Koopman layer would enable joint forecasting and control for cyber–physical systems, while exploring richer backbones (e.g., state–space models with Koopman regularisation, graph-based or spatio-temporal Transformers) could further broaden applicability. Finally, scaling `Learnable-DeepKoopFormer` to larger benchmarks and online or continual-learning scenarios would help assess how learnable Koopman operators behave under persistent distribution shift. We view this work as a step toward a principled synthesis of operator-theoretic dynamics and modern deep forecasting, and anticipate that Koopman-enhanced architectures will become a useful building block in the broader toolbox of interpretable, stable sequence models.

## APPENDIX

### REFERENCES

- [1] J. D. Croston, “Forecasting and stock control for intermittent demands,” *Journal of the Operational Research Society*, vol. 23, pp. 289–303, Sep 1972.
- [2] R. Wen, K. Torkkola, B. Narayanaswamy, and D. Madeka, “A multi-horizon quantile recurrent forecaster,” *arXiv preprint arXiv:1711.11053*, 2017.
- [3] D. Salinas, V. Flunkert, J. Gasthaus, and T. Januschowski, “DeepAR: Probabilistic forecasting with autoregressive recurrent networks,” *International Journal of Forecasting*, vol. 36, no. 3, pp. 1181–1191, 2020.
- [4] Y. Lv, Y. Duan, W. Kang, Z. Li, and F.-Y. Wang, “Traffic flow prediction with big data: A deep learning approach,” *IEEE Transactions on Intelligent Transportation Systems*, vol. 16, no. 2, pp. 865–873, 2014.
- [5] Y. Li, R. Yu, C. Shahabi, and Y. Liu, “Diffusion convolutional recurrent neural network: Data-driven traffic forecasting,” in *International Conference on Learning Representations*, 2018.
- [6] I. Dimoulkas, P. Mazidi, and L. Herre, “Neural networks for GEFCom2017 probabilistic load forecasting,” *International Journal of Forecasting*, vol. 35, no. 4, pp. 1409 – 1423, 2019.
- [7] H. Saxena, O. Aponte, and K. T. McConky, “A hybrid machine learning model for forecasting a billing period’s peak electric load days,” *International Journal of Forecasting*, vol. 35, no. 4, pp. 1288 – 1303, 2019.
- [8] A. Forootani, D. Esmaeili Aliabadi, and D. T. n, “Climate aware deep neural networks (cadnn) for wind power simulation,” *Array*, vol. 28, p. 100534, 2025.
- [9] L. A. Callot, A. B. Kock, and M. C. Medeiros, “Modeling and forecasting large realized covariance matrices and portfolio choice,” *Journal of Applied Econometrics*, vol. 32, no. 1, pp. 140–158, 2017.
- [10] X. Yan, W. Zhang, L. Ma, W. Liu, and Q. Wu, “Parsimonious quantile regression of financial asset tail dynamics via sequential learning,” *Advances in Neural Information Processing Systems*, vol. 31, 2018.
- [11] R. J. Hyndman and G. Athanasopoulos, *Forecasting: principles and practice*. OTexts, 2018.
- [12] S. Hochreiter and J. Schmidhuber, “Long short-term memory,” *Neural Computation*, vol. 9, no. 8, pp. 1735–1780, 1997.
- [13] Y. LeCun and Y. Bengio, “Convolutional networks for images, speech, and time series,” *The handbook of brain theory and neural networks*, vol. 3361, no. 10, 1995.
- [14] S. Bai, J. Z. Kolter, and V. Koltun, “An empirical evaluation of generic convolutional and recurrent networks for sequence modeling,” *arXiv preprint arXiv:1803.01271*, 2018.
- [15] H. Wu, J. Xu, J. Wang, and M. Long, “Autoformer: Decomposition transformers with Auto-Correlation for long-term series forecasting,” in *NeurIPS*, 2021.
- [16] H. Zhou, S. Zhang, J. Peng, S. Zhang, J. Li, H. Xiong, and W. Zhang, “Informer: Beyond efficient transformer for long sequence time-series forecasting,” in *AAAI*, 2021.

**Algorithm 1** DeepKoopFormer for Multivariate Time Series Forecasting

Input: Multivariate time series  $\{x_t\}_{t=1}^T$ , context length  $P$ , forecast horizon  $H$

Output: Predicted sequence  $\hat{Y} = [\hat{x}_{t+P}, \dots, \hat{x}_{t+P+H-1}]$

1: Data Preparation:

- For each valid  $t$ , construct:

$$X_t = [x_t, \dots, x_{t+P-1}] \in \mathbb{R}^{P \times d},$$

$$Y_t = [x_{t+P}, \dots, x_{t+P+H-1}] \in \mathbb{R}^{H \times d}.$$

2: Latent Encoding:

- Compute latent vector:  $z_t = \mathcal{E}_\theta(X_t)$ , where  $\mathcal{E}_\theta$  is a Transformer-based encoder with positional encoding.

3: Koopman Operator Evolution:

- Propagate the latent state:  $z_{t+1} = \mathcal{K}_\phi z_t$ .
- $\mathcal{K}_\phi$  is parameterized as:  $\mathcal{K}_\phi = U_\phi \text{diag}(\Sigma_\phi) V_\phi^\top$ , where  $U_\phi, V_\phi$  are orthogonal matrices,  $\Sigma_\phi = \sigma(S) \rho_{\max}$ , where  $\sigma(\cdot)$  is the sigmoid function,  $S$  raw parameters, and  $\rho_{\max} < 1$ .

4: Output Decoding (Direct  $H$ -Step Forecast):

- Map the refined latent state to the  $H$ -step forecast via a linear decoder:  $\hat{y}_t = \mathcal{D}_\varphi(z_{t+1}) \in \mathbb{R}^{H \cdot d}$ , where  $\mathcal{D}_\varphi$  is implemented as a fully connected linear layer.
- Reshape to obtain the forecast sequence:

$$\hat{Y}_t = \text{reshape}(\hat{y}_t, H, d) = [\hat{x}_{t+P}, \dots, \hat{x}_{t+P+H-1}] \in \mathbb{R}^{H \times d}.$$

5: Loss Function:

$$\mathcal{L} = \|\hat{Y}_t - Y_t\|^2 + \lambda \cdot \text{ReLU}(\|z_{t+1}\|^2 - \|z_t\|^2).$$

6: Optimization: Train parameters  $(\theta, \phi, \mathcal{K}_\phi)$  end-to-end with Adam.

7: Inference: At test time, given a context window  $X_t$ , compute  $z_t = \mathcal{E}_\theta(X_t)$ ,  $z_{t+1} = \mathcal{K}_\phi z_t$ , and obtain the  $H$ -step forecast in a single forward pass as

$$\hat{y}_t = \mathcal{D}_\varphi(z_{t+1}), \quad \hat{Y}_t = \text{reshape}(\hat{y}_t, H, d).$$

[17] Y. Nie, N. H. Nguyen, P. Sinthong, and J. Kalagnanam, “A time series is worth 64 words: Long-term forecasting with transformers,” *arXiv preprint arXiv:2211.14730*, 2022.

[18] A. Vaswani, N. Shazeer, N. Parmar, J. Uszkoreit, L. Jones, A. N. Gomez, Ł. Kaiser, and I. Polosukhin, “Attention is all you need,” in *Advances in Neural Information Processing Systems*, pp. 5998–6008, 2017.

[19] S. Smyl, “A hybrid method of exponential smoothing and recurrent neural networks for time series forecasting,” *International Journal of Forecasting*, vol. 36, no. 1, pp. 75–85, 2020.

[20] S. Makridakis, E. Spiliotis, V. Assimakopoulos, Z. Chen, A. Gaba, I. Tsetlin, and R. L. Winkler, “The m5 uncertainty competition: Results, findings and conclusions,” *International Journal of Forecasting*, 2021.

[21] H. Zhou, S. Zhang, J. Peng, S. Zhang, J. Li, H. Xiong, and W. Zhang, “Informer: Beyond efficient transformer for long sequence time-series forecasting,” in *The Thirty-Fifth AAAI Conference on Artificial Intelligence*, vol. 35, pp. 11106–11115, 2021.

[22] H. Wu, J. Xu, J. Wang, and M. Long, “Autoformer: Decomposition transformers with Auto-Correlation for long-term series forecasting,” in *Advances in Neural Information Processing Systems*, 2021.

[23] T. Zhou, Z. Ma, Q. Wen, X. Wang, L. Sun, and R. Jin, “FEDformer: Frequency enhanced decomposed transformer for long-term series fore-

casting,” in *Proc. 39th International Conference on Machine Learning*, 2022.

[24] T. Zhou, Z. Ma, Q. Wen, X. Wang, L. Sun, and R. Jin, “FEDformer: Frequency enhanced decomposed transformer for long-term series forecasting,” in *ICML*, 2022.

[25] S. Liu, H. Yu, C. Liao, J. Li, W. Lin, A. X. Liu, and S. Dustdar, “Pyraformer: Low-complexity pyramidal attention for long-range time series modeling and forecasting,” in *International Conference on Learning Representations*, 2022.

[26] S. Liu, H. Yu, C. Liao, J. Li, W. Lin, A. X. Liu, and S. Dustdar, “Pyraformer: Low-complexity pyramidal attention for long-range time series modeling and forecasting,” in *ICLR*, 2021.

[27] Y. Zheng, Q. Liu, E. Chen, Y. Ge, and J. L. Zhao, “Time series classification using multi-channels deep convolutional neural networks,” in *International conference on web-age information management*, pp. 298–310, Springer, 2014.

[28] A. Zeng, M. Chen, L. Zhang, and Q. Xu, “Are transformers effective for time series forecasting?,” *arXiv preprint arXiv:2205.13504*, 2022.

[29] A. Zeng, M. Chen, L. Zhang, and Q. Xu, “Are transformers effective for time series forecasting?,” in *Proceedings of the AAAI conference on artificial intelligence*, vol. 37, pp. 11121–11128, 2023.

[30] V. Kuznetsov and M. Mohri, “Discrepancy-based theory and algorithms for forecasting non-stationary time series,” *Annals of Mathematics and Artificial Intelligence*, vol. 88, no. 4, pp. 367–399, 2020.

[31] Y. Liu, H. Wu, J. Wang, and M. Long, “Non-stationary transformers: Rethinking the stationarity in time series forecasting,” *arXiv preprint arXiv:2205.14415*, 2022.

[32] T. Kim, J. Kim, Y. Tae, C. Park, J.-H. Choi, and J. Choo, “Reversible instance normalization for accurate time-series forecasting against distribution shift,” in *ICLR*, 2022.

[33] Y. Wang, A. Smola, D. Maddix, J. Gasthaus, D. Foster, and T. Januschowski, “Deep factors for forecasting,” in *International Conference on Machine Learning*, pp. 6607–6617, 2019.

[34] R. Sen, H.-F. Yu, and I. S. Dhillon, “Think globally, act locally: A deep neural network approach to high-dimensional time series forecasting,” *Advances in Neural Information Processing Systems*, vol. 32, 2019.

[35] R. T. Chen, Y. Rubanova, J. Bettencourt, and D. K. Duvenaud, “Neural ordinary differential equations,” *Advances in Neural Information Processing Systems*, vol. 31, 2018.

[36] F.-X. Vialard, R. Kwitt, S. Wei, and M. Niethammer, “A shooting formulation of deep learning,” in *Advances in Neural Information Processing Systems*, 2020.

[37] I. Mezić, *Spectral operator methods in dynamical systems: Theory and applications*. Springer, 2017.

[38] M. Khosravi, “Representer theorem for learning koopman operators,” *IEEE Transactions on Automatic Control*, vol. 68, no. 5, pp. 2995–3010, 2023.

[39] M. O. Williams, I. G. Kevrekidis, and C. W. Rowley, “A data-driven approximation of the koopman operator: Extending dynamic mode decomposition,” *Journal of Nonlinear Science*, vol. 25, pp. 1307–1346, 2015.

[40] J. N. Kutz, S. L. Brunton, B. W. Brunton, and J. L. Proctor, *Dynamic Mode Decomposition: Data-Driven Modeling of Complex Systems*. SIAM, 2016.

[41] J. Drgona, A. Tuor, S. Vasishth, and D. Vrabie, “Dissipative deep neural dynamical systems,” *IEEE Open Journal of Control Systems*, vol. 1, pp. 100–112, 2022.

[42] E. Skomski, S. Vasishth, C. Wight, A. Tuor, J. Drgona, and D. Vrabie, “Constrained block nonlinear neural dynamical models,” in *2021 American Control Conference (ACC)*, pp. 3993–4000, 2021.

[43] J. Drgona, S. Mukherjee, J. Zhang, F. Liu, and M. Halappanavar, “On the stochastic stability of deep markov models,” in *Advances in Neural Information Processing Systems* (M. Ranzato, A. Beygelzimer, Y. Dauphin, P. Liang, and J. W. Vaughan, eds.), vol. 34, pp. 24033–24047, Curran Associates, Inc., 2021.

[44] B. Lusch, J. N. Kutz, and S. L. Brunton, “Deep learning for universal linear embeddings of nonlinear dynamics,” *Nature Communications*, vol. 9, p. 4950, Nov. 2018.

[45] E. Yeung, S. Kundu, and N. Hudas, “Learning deep neural network representations for Koopman operators of nonlinear dynamical systems,” in *2019 American Control Conference (ACC)*, pp. 4832–4839, 2019.

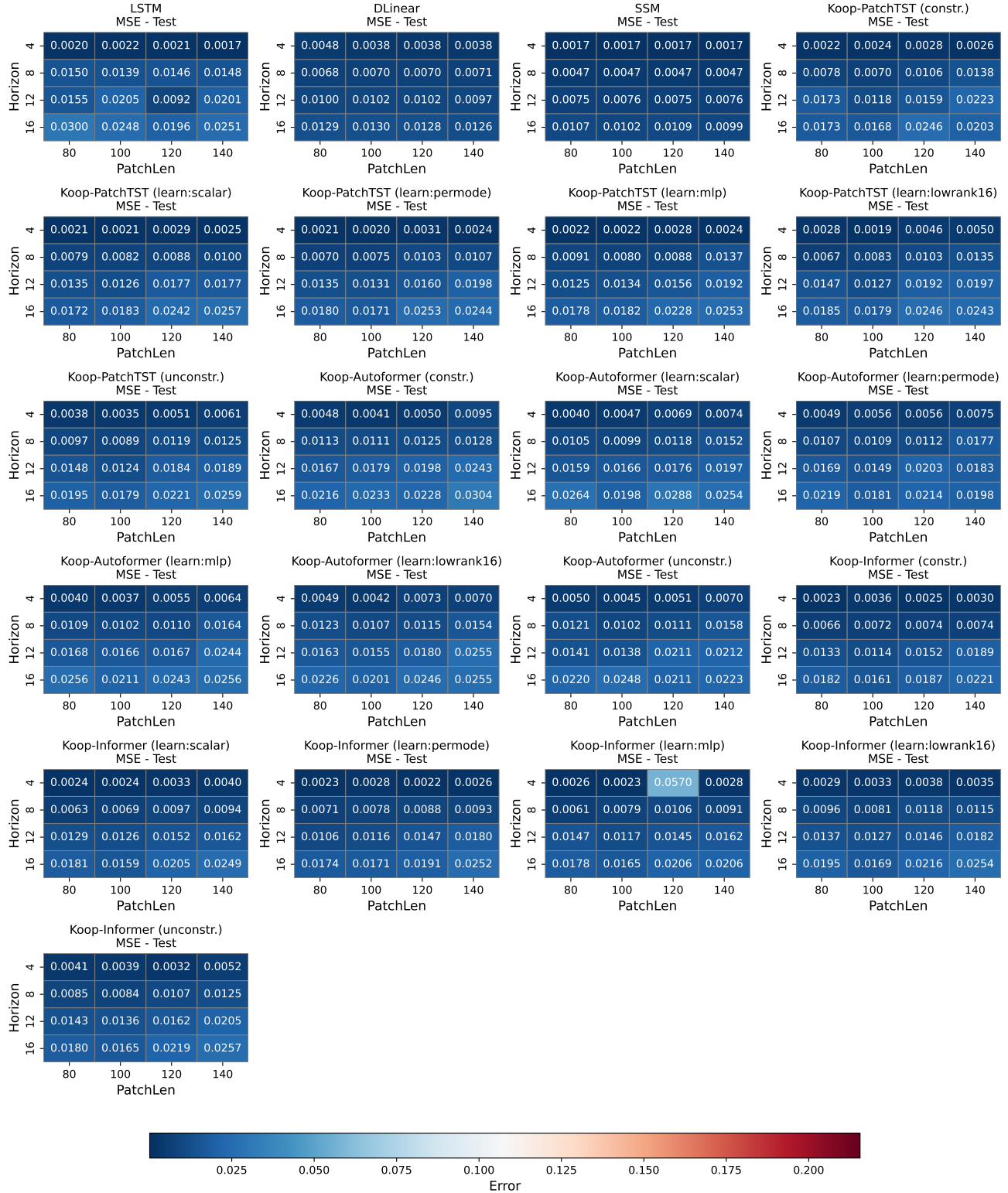
[46] N. Takeishi, Y. Kawahara, and T. Yairi, “Learning Koopman invariant subspaces for dynamic mode decomposition,” in *Advances in Neural Information Processing Systems* (I. Guyon, U. V. Luxburg, S. Bengio, H. Wallach, R. Fergus, S. Vishwanathan, and R. Garnett, eds.), vol. 30, Curran Associates, Inc., 2017.

- [47] B. Lusch, J. N. Kutz, and S. L. Brunton, “Deep learning for universal linear embeddings of nonlinear dynamics,” *Nature communications*, vol. 9, no. 1, p. 4950, 2018.
- [48] O. Azencot, N. B. Erichson, V. Lin, and M. Mahoney, “Forecasting sequential data using consistent koopman autoencoders,” in *International Conference on Machine Learning*, pp. 475–485, PMLR, 2020.
- [49] J. Morton, A. Jameson, M. J. Kochenderfer, and F. Witherden, “Deep dynamical modeling and control of unsteady fluid flows,” *Advances in Neural Information Processing Systems*, vol. 31, 2018.
- [50] N. Takeishi, Y. Kawahara, and T. Yairi, “Learning koopman invariant subspaces for dynamic mode decomposition,” *Advances in neural information processing systems*, vol. 30, 2017.
- [51] S. L. Brunton, M. Budisic, E. Kaiser, and J. N. Kutz, “Modern koopman theory for dynamical systems,” *arXiv preprint arXiv:2102.12086*, 2021.
- [52] A. Forootani, M. Khosravi, and M. Barati, “Deepkoopformer: A koopman enhanced transformer based architecture for time series forecasting,” *arXiv preprint arXiv:2508.02616*, 2025.
- [53] G. Karniadakis, I. Kevrekidis, L. Lu, P. Perdikaris, S. Wang, and L. Yang, “Physics-informed machine learning,” *Nature Reviews Physics*, vol. 3, pp. 422–440, June 2021. Publisher Copyright: © 2021, Springer Nature Limited.
- [54] T. X. Nghiem, J. Drgoňa, C. Jones, Z. Nagy, R. Schwan, B. Dey, A. Chakrabarty, S. Di Cairano, J. A. Paulson, A. Carron, M. N. Zeilinger, W. Shaw Cortez, and D. L. Vrabie, “Physics-informed machine learning for modeling and control of dynamical systems,” in *2023 American Control Conference (ACC)*, pp. 3735–3750, 2023.
- [55] S. L. Brunton, B. W. Brunton, J. L. Proctor, and J. Kutz, “Koopman invariant subspaces and finite linear representations of nonlinear dynamical systems for control,” *PLoS ONE*, vol. 11, no. 2, p. e0150171, 2016.
- [56] M. Korda and I. Mezić, “Linear predictors for nonlinear dynamical systems: Koopman operator meets model predictive control,” *arXiv:1611.03537*, 2016.
- [57] A. Gu, I. Johnson, K. Goel, K. Saab, T. Dao, A. Rudra, and C. Ré, “Combining recurrent, convolutional, and continuous-time models with linear state-space layers,” *NeurIPS*, 2021.
- [58] D. P. Kingma and J. Ba, “Adam: A method for stochastic optimization,” 2015.
- [59] P.-A. Absil, R. Mahony, and R. Sepulchre, *Optimization algorithms on matrix manifolds*. Princeton University Press, 2008.
- [60] M. M. Lin, “Discrete eckart–young theorem for integer matrices,” *SIAM journal on matrix analysis and applications*, vol. 32, no. 4, pp. 1367–1382, 2011.
- [61] A. Gu, K. Goel, and C. Ré, “Efficiently modeling long sequences with structured state spaces,” *arXiv preprint arXiv:2111.00396*, 2021.
- [62] J. T. Smith, A. Warrington, and S. W. Linderman, “Simplified state space layers for sequence modeling,” *arXiv preprint arXiv:2208.04933*, 2022.
- [63] J. D. Hamilton, *Time series analysis*. Princeton university press, 2020.
- [64] E. K. Makula and B. Zhou, “Coupled model intercomparison project phase 6 evaluation and projection of east african precipitation,” *International Journal of Climatology*, vol. 42, no. 4, pp. 2398–2412, 2022.
- [65] H. Hersbach, B. Bell, P. Berrisford, S. Hirahara, A. Horányi, J. Muñoz-Sabater, J. Nicolas, C. Peubey, R. Radu, D. Schepers, *et al.*, “The era5 global reanalysis,” *Quarterly journal of the royal meteorological society*, vol. 146, no. 730, pp. 1999–2049, 2020.

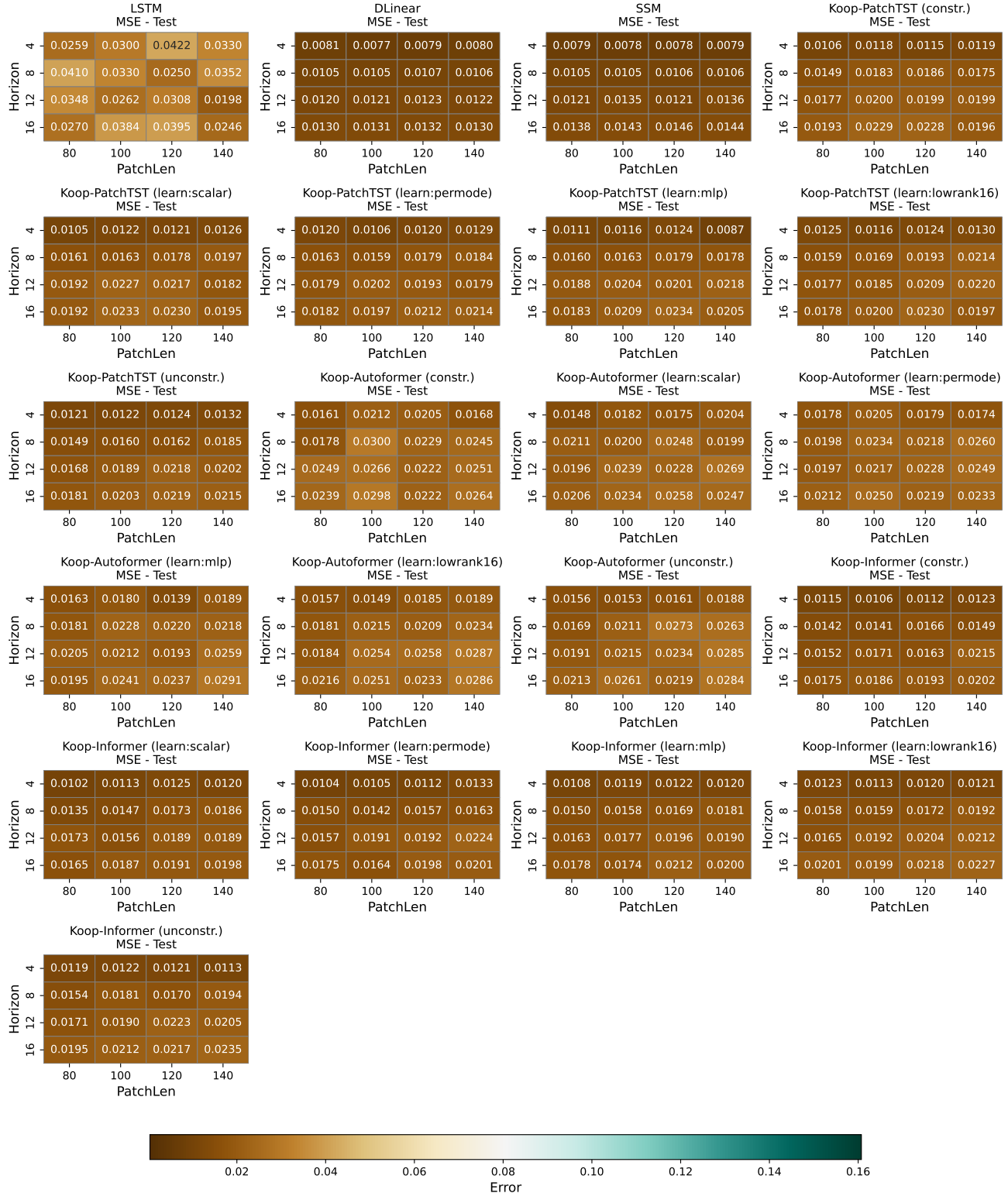
## APPENDIX

- A. Pressure Surface MSE Test
- B. Wind Speed MSE Test
- C. Cryptocurrency
- D. Energy Systems MSE Test
- E. ERA5 Wind Speed MSE Test

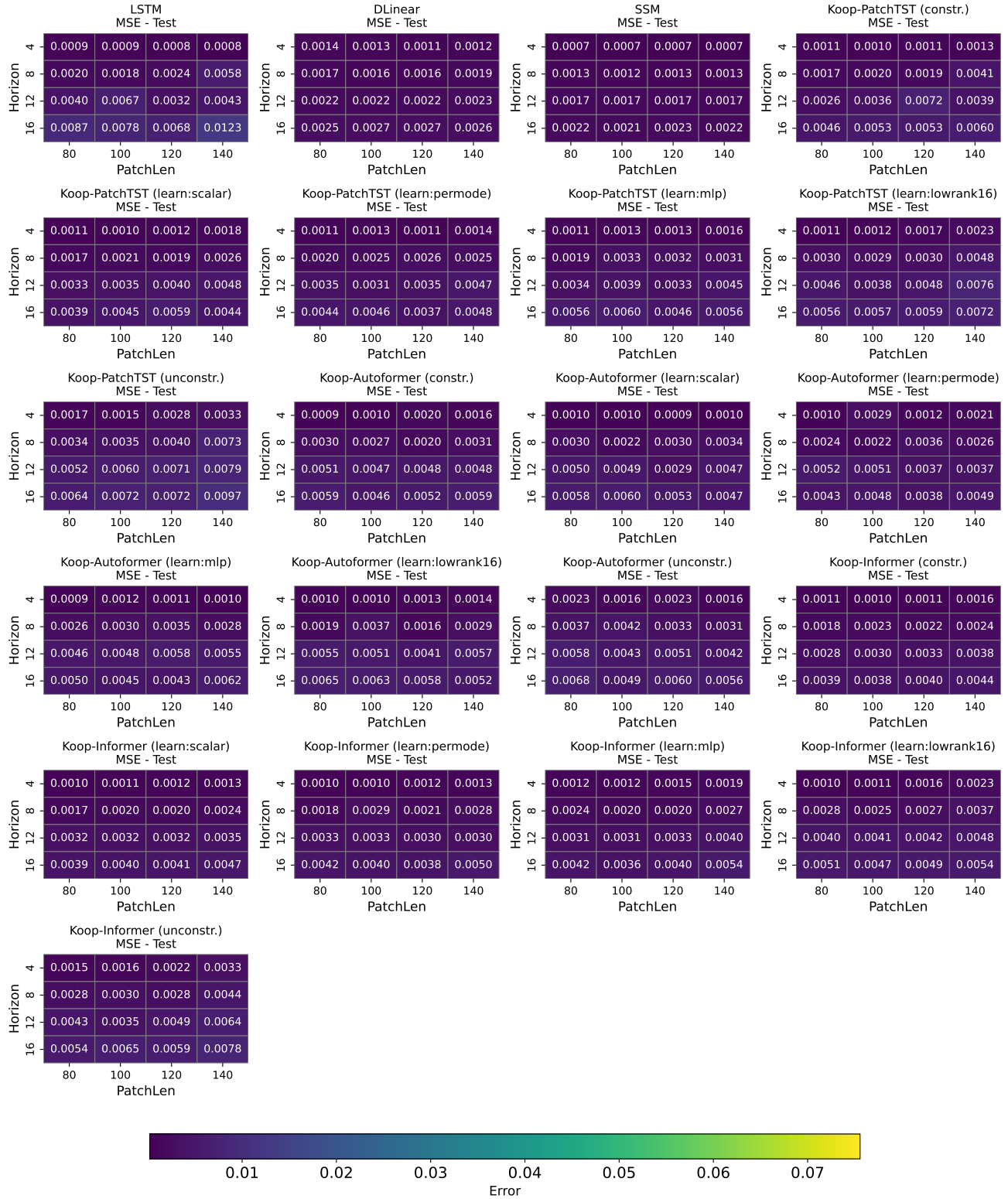
**DeepKoopFormer: MSE (Test set)- Pressure Surface**  
**Constrained vs learnable vs unconstrained Koopman + LSTM/DLinear/SSM baselines**



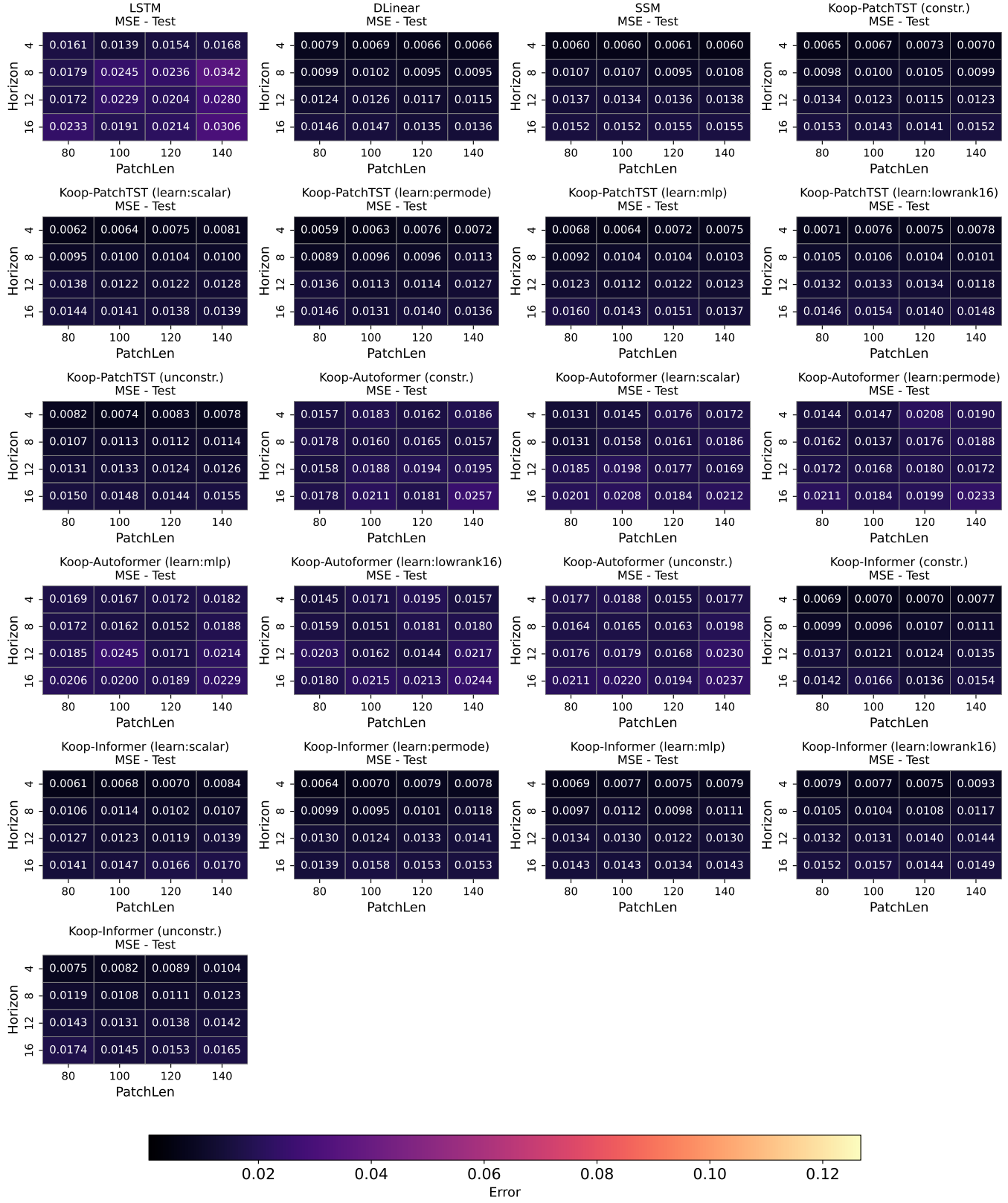
**DeepKoopFormer: MSE (Test set)- Wind Speed**  
**Constrained vs learnable vs unconstrained Koopman + LSTM/DLinear/SSM baselines**



**DeepKoopFormer: MSE (Test set)- Cryptocurrency**  
**Constrained vs learnable vs unconstrained Koopman + LSTM/DLinear/SSM baselines**



**DeepKoopFormer: MSE (Test set)- Energy Systems**  
**Constrained vs learnable vs unconstrained Koopman + LSTM/DLinear/SSM baselines**



**DeepKoopFormer: MSE (Test set)- ERA5 Wind Speed**  
**Constrained vs learnable vs unconstrained Koopman + LSTM/DLinear/SSM baselines**

